



Inhibitors of the *Neisseria meningitidis* PilF ATPase provoke type IV pilus disassembly

Flore Aubey, Jean-Philippe Corre, Youxin Kong, Ximing Xu, Dorian Obino,
Sylvie Goussard, Catherine Lapeyrere, Judith Souphron, Cedric Couturier,
Stéphane Renard, et al.

► To cite this version:

Flore Aubey, Jean-Philippe Corre, Youxin Kong, Ximing Xu, Dorian Obino, et al.. Inhibitors of the *Neisseria meningitidis* PilF ATPase provoke type IV pilus disassembly. Proceedings of the National Academy of Sciences of the United States of America, 2019, 116 (17), pp.8481-8486. 10.1073/pnas.1817757116 . pasteur-03100484

HAL Id: pasteur-03100484

<https://pasteur.hal.science/pasteur-03100484>

Submitted on 18 Jan 2021

HAL is a multi-disciplinary open access archive for the deposit and dissemination of scientific research documents, whether they are published or not. The documents may come from teaching and research institutions in France or abroad, or from public or private research centers.

L'archive ouverte pluridisciplinaire **HAL**, est destinée au dépôt et à la diffusion de documents scientifiques de niveau recherche, publiés ou non, émanant des établissements d'enseignement et de recherche français ou étrangers, des laboratoires publics ou privés.

1 *Classification:* BIOLOGICAL SCIENCES, Microbiology

2
3 **Inhibitors of the *Neisseria meningitidis* PilF ATPase provoke**
4 **type IV pilus disassembly**
5

6 Short title: *Inhibitors of Neisseria adhesion*

7
8 Flore Aubey^{a,1}, Jean-Philippe Corre^{a,1}, Youxin Kong^{a,1}, Ximing Xu^{a,1}, Dorian Obino^a, Sylvie
9 Goussard^a, Catherine Lapeyrere^b, Judith Souphron^a, Cedric Couturier^b, Stéphane
10 Renard^b and Guillaume Duménil^{a,2}

11
12 **Affiliations**

13 ^a Pathogenesis of Vascular Infections, Department of Cell Biology and Infection, Institut Pasteur,
14 INSERM, 75015, Paris, France.

15 ^b Sanofi, Department of Infectious Disease, 69280, Marcy l'Etoile, France

16 ¹ These authors contributed equally to this work, names are indicated in alphabetical order.

17 ² To whom correspondence may be addressed. Guillaume Duménil, Pathogenesis of Vascular
18 Infections, Department of Cell Biology and Infection, Institut Pasteur, INSERM, 28 rue du Docteur
19 Roux, 75015, Paris, France, +33144389383, guillaume.dumenil@pasteur.fr

20
21 **Keywords:** Type four pili; Meningitis; Sepsis; Adhesion; Endothelium; *Neisseria*; Inhibitors;
22 **Bacteria**

Abstract

Despite the availability of antibiotics and vaccines, *Neisseria meningitidis* remains a major cause of meningitis and sepsis in humans. Due to its extracellular lifestyle, bacterial adhesion to host cells constitutes an attractive therapeutic target. Here we present a high-throughput microscopy-based approach that allowed the identification of compounds able to decrease type IV pilus-mediated interaction of bacteria with endothelial cells in absence of bacterial or host cell toxicity. Compounds specifically inhibit the PilF ATPase enzymatic activity that powers type IV pilus extension but remain inefficient on the ATPase that promotes pilus retraction thus leading to rapid pilus disappearance from the bacterial surface and loss of pili-mediated functions. Structure activity relationship of the most active compound identifies specific moieties required for the activity of this compound and highlights its specificity. This study therefore provides the first compounds targeting pilus biogenesis, thereby inhibiting bacterial adhesion, and pave the way for a novel therapeutic option for meningococcal infections.

Significance Statement

A number of multimeric protein nanomachines such as secretion systems and surface appendages allow bacteria to adapt and survive in a variety of environments. Type IV pili are one of the most common of such machineries. The human pathogen *Neisseria meningitidis* uses type IV pili to colonize blood vessels and cause disease. Here, we identify compounds that trigger the rapid retraction of type IV pili. Furthermore, we identify the target of these small molecules as an ATPase known as PilF among the 20 proteins involved in pilus assembly and function. This study paves the way for an innovative treatment strategy for different pathogens and provides new information on the molecular mechanisms driving the assembly and dynamics of bacterial machineries.

Introduction

Neisseria meningitidis is a pathogenic bacterium responsible for sepsis and meningitis that remain a major concern in emergency wards despite the availability of antibiotics (1). The human nasopharynx is the only known natural reservoir for *N. meningitidis* and transmission to new hosts occurs directly via droplets (2). This bacterium colonizes the naso-oropharynx of a substantial proportion of the population, 3 to 30% depending on the study (3). Pathology is initiated when bacteria reach the bloodstream where they survive and proliferate. When the bacteremia is not cleared rapidly, two severe although fairly distinct disease manifestations can develop: sepsis or meningitis if bacteria also crossed the blood-brain barrier (1). Fulminant meningococcal sepsis, subsequent to septicemia, is the most devastating form of sepsis with a mortality rate varying from 20 to 30% despite antimicrobial treatment and medical care. It is characterized by a rapidly evolving septic shock, disseminated intravascular coagulation (DIC) and skin haemorrhage (*purpura fulminans*).

Because of the rapid evolution of the disease and the severity of the symptoms, industrial and basic research efforts have focused on the design of vaccine strategies (4). Conjugated polysaccharide vaccines have been very successful for specific serogroups, but these approaches also show certain limits due to the diversity and variability of surface structures in *Neisseria meningitidis* (5, 6). Serogroup B which represents the majority of cases in most other countries is also a particular problem because its capsular polysaccharide is similar to one found in humans (7). The reverse vaccinology approach addressed this issue by generating the Bexsero vaccine (8) combining several surface structures but its efficiency is still under evaluation and it will always be efficient on a subset of strains only (9). In addition to these efforts in the field of prevention, new therapeutic approaches should thus also be considered.

To treat infections more efficiently, there is a need for a paradigm shift. It seems unlikely that a super antibiotic with extended spectrum that can replace existing therapies without any of the side

73 effects generally associated with antibiotics will ever arise. New classes of anti-infectious
74 compounds need to be found to instigate this paradigm shift. To reach this goal, one must
75 investigate an avenue that remains largely unexplored in terms of medicinal chemistry: host-
76 bacteria interactions and virulence factors (10). By targeting these determinants of infection, these
77 new therapeutical approaches would greatly enhance classical antibacterial treatments and
78 improve therapy outcome and patient welfare.

79 Central virulent properties of *N. meningitidis* include adhesion to host cells (11), and this
80 constitutes an original and attractive target for treatments. Adhesion of *N. meningitidis* to human
81 cells is a key step in the life cycle of this organism by allowing nasopharynx colonization and
82 adhesion to endothelial cells, each of these events promoting blood and brain colonization by the
83 bacteria. Neisserial type IV pili (Tfp) have long been recognized as playing an essential role in the
84 pathogenesis of *N. meningitidis*, and primary cultures of clinical isolates of pathogenic *Neisseria*
85 are invariably piliated (12, 13). In a humanized animal model type IV pili were shown to be
86 responsible for adhesion along the endothelium and to trigger the vascular damages observed
87 during infection, including loss of vascular integrity, coagulation and congestion (13, 14). In
88 addition to type IV pili, *Neisseria meningitidis* expresses several other transmembrane adhesins,
89 the most studied being the Opa family of adhesins (15). These additional adhesins tune the
90 interaction with host cells by promoting host-pathogen intimate interactions, triggering intracellular
91 signalling events and favouring intracellular invasion. Adhesion is thus a key feature of *N.*
92 *meningitidis* pathogenesis that constitutes a promising therapeutic target.

93 In this study, we identified compounds that inhibit the adhesion of *N. meningitidis* to host cells by
94 screening a library of compounds and identified their mode of action down to the molecular and
95 chemical level.

Results

Identification of compounds decreasing *Neisseria meningitidis* adhesion to human endothelial cells

Adhesion to the human endothelium can be recapitulated *in vitro* using cultured endothelial cells. Bacteria rapidly adhere as individual diplococci to the host cell surface and subsequently divide, forming tight roughly circular aggregates, termed microcolonies, which can reach 10-20 μm in diameter within 2-4 hours. Thus, the size and number of these microcolonies as visualized by fluorescence microscopy represent good markers for the ability of bacteria to adhere to endothelial cells and proliferate on their surface. A microscopy-based high-throughput screening approach was therefore selected and optimized to identify compounds that block *N. meningitidis* adhesion onto endothelial cells. Monolayers of primary human umbilical vein endothelial cells (HUVEC) in 384-well plates were pre-treated with 1 μM of each compound for 30 minutes prior to be infected with *N. meningitidis*. Non-adhering bacteria were washed-out following a 30-min incubation and adhering bacteria were allowed to proliferate in the presence of the compounds for 4 hours (Fig. 1A). A library containing 2,239 compounds was used to block adhesion. This library contains a combination of FDA approved drugs, inhibitors of Kegg pathways, kinase inhibitors and a selection of Sanofi lead compounds (Fig. 1B). Microcolonies were visualized by labelling bacteria with an antibody directed against capsular antigens, and host cells were detected with a DNA labelling dye (Hoechst 33342). Images were then segmented and analysed, allowing extraction of several parameters such as microcolony size and number but also cellular toxicity (number of nuclei per field of view) (Fig. 1C). Compound activity was expressed as a percentage of adhesion inhibition relative to positive (non-infected cells, 100 % inhibition) and negative (no compound, 0% inhibition) controls in each plate of the two replicates. Among the tested compounds, 163 hits were selected based on their effective inhibition of bacterial adhesion ($\geq 60\%$) and low cellular toxicity ($\leq 10\%$) (Fig. 1D and SI Appendix Table S1). 72 compounds were confirmed in a validation assay and 59

of them (because of availability limitation) were further analysed using a dose response approach ranging from 30 μ M to 1 nM. First, the potential of each compound to inhibit the formation of bacterial colonies was used to calculate their half maximal inhibitory concentration (IC₅₀, SI Appendix Table S2). Then, the cellular toxicity of each compound was evaluated on HepG2 cells and their median toxic concentration (TC₅₀) was determined (SI Appendix Table S2). Correlation analysis of IC₅₀ and TC₅₀ highlighted two main groups of compounds: one including compounds showing intermediate cellular toxicity but very potent inhibition of bacterial adhesion (Fig. 2A, light red) and a second group of compounds harbouring a lower cellular toxicity but also a lower inhibitory efficiency (Fig. 2A, light grey). We therefore selected the best compounds of each group that will be referred to as A, B and C, hereafter (Fig. 2A, red dots and SI Appendix Table S2) and evaluated their cellular toxicity on both THP1 and HepG2 cells (SI Appendix Fig. S1). Their chemical structures are indicated on figure 2B. Dose response curves confirmed that compound A was the most active with an IC₅₀ of 7.20×10^{-9} M, followed by B with a value of 1.73×10^{-8} M, and C was slightly less active with a value of 2.66×10^{-7} M (Fig. 2C and SI Appendix Table S2). Despite the exclusion from the screening analysis of compounds with known bactericidal activity, the effects of the three selected compounds could be indirectly due to an alteration of bacterial viability. We therefore tested this potential effect by performing growth curves in the presence of the compounds. None of the three compounds had any effect on bacterial growth at a concentration of 1 μ M (Fig. 2D). This microscopy-based screening approach thus allowed us to identify new compounds that can reduce the number of bacteria adhering to human endothelial cells without affecting bacterial viability.

Compounds affect type IV pili display on the bacterial surface

To further validate the effects of the three compounds in conditions closer to a therapeutic application, their ability to induce the detachment of adhering bacteria was then evaluated. Bacteria were allowed to adhere at the surface of endothelial cells and then proliferate for 4 hours

147 before adding the compounds for 30 minutes, and bacterial adhesion was evaluated by counting
148 cell-associated colony forming units (CFU, Fig. 3A). In line with our screening data, this assay
149 confirmed the efficiency of the selected compounds and showed that they can act after bacterial
150 adhesion and proliferation. Compound B was the most potent in detaching previously adhering
151 bacteria with a five-fold decrease, whereas compounds A and C were slightly less efficient (Fig.
152 3B). The non-piliated strain *pilD* defective for adhesion to the host cells was used to determine a
153 base-line of bacterial adhesion and showed that the effect of the compounds is not complete (Fig.
154 3B). The compounds identified in the screen are thus efficient at detaching previously adhering
155 bacteria, pointing to an effect on adhesion itself.

156 Adhesion of *Neisseria meningitidis* to human endothelial cells is largely mediated by Tfp,
157 suggesting that the compounds identified in the screen could affect the function or assembly of
158 these structures. Since Tfp carry several other functions, including bacterial auto-aggregation, a
159 prediction is that bacterial aggregation would be affected by compounds that affect pilus assembly.
160 Bacterial aggregates in suspension (in the absence of endothelial cells) generated by GFP-
161 expressing *N. meningitidis* were treated with compound B and observed by video-microscopy (Fig.
162 3C). Addition of the compound led to a rapid disaggregation of the bacteria followed by their
163 progressive diffusion away from the aggregate centre. The effect was detectable as early as 30
164 seconds following compound B addition. Inhibition of bacterial aggregation was further quantified
165 using a 4x magnification lens and automated counting of aggregate number in wells of 96-well
166 plates. Using this approach, we first evaluated the effect of the three compounds on the ability of
167 individual bacteria to form aggregates (Fig. 3D). In these conditions, compounds A and B
168 completely blocked aggregate formation whereas compound C had only a partial effect (Fig. 3D).
169 We then evaluated the ability of a 30-minute treatment with the compounds to disaggregate
170 preformed aggregates (Fig. 3E). In absence of compounds, the number of bacteria engaged within
171 an aggregate increased over the 30-minute period (DMSO). In contrast, compounds A and B were
172 extremely efficient in disaggregating preformed bacterial aggregates while compound C only

showed a partial effect (Fig. 3E). Of note, compound B was also able to prevent the auto-aggregation of *N. gonorrhoeae* and induced the disaggregation of preformed gonococcal aggregates (Fig. 3D and E, left panels). These results show that the three compounds identified in the screen affect the bacterial aggregation in addition to adhesion, most probably by altering the function or biogenesis of type IV pili.

We therefore evaluated whether bacterial treatment with the compounds is associated with a decrease in the amount of bacterial Tfp. The amount of Tfp displayed by the bacteria can be assessed using an ELISA-based approach on whole bacteria immobilized in 96-well plates and probed with an anti-Tfp antibody. This assay revealed that the three compounds affected bacterial piliation at various levels (Fig. 3F), with compound B being again the most efficient with a five-fold decrease in piliation. This effect was also visible when immunostaining Tfp (Fig. 3G). Although the effect of compounds A and C on piliation might seem relatively mild, we have previously shown that minor reductions in piliation levels strongly affect Tfp-mediated functions (16). Altogether, it can be concluded from these results that the compounds identified in the screen exert their effect by decreasing the surface expression levels of bacterial type IV pili.

Structure activity relationship of compound B

Since compound B was the most efficient, we decided to establish the structure activity relationship (SAR) of this compound. To this end, we characterized the effect on bacterial aggregation of a series of 49 compounds closely related to compound B. As described in figure 3D, individual bacteria were treated with 0.1 μ M of each derivative and incubated 30 min to form aggregates. Of note, at this concentration, treatment with compound B only led to the partial inhibition of bacterial aggregation (Fig. 4A), giving the opportunity to highlight derivatives with an increased (or decreased) activity. While most derivatives showed a reduced ability to inhibit bacterial aggregation (Fig. 4B, light red), a few of them displayed a slightly higher effect (Fig. 4B, light green) than compound B, allowing us to establish the SAR (SI Appendix Table S3). Therefore,

the relative importance of the three main groups forming compound B, the 2,4-dimethoxybenzene, the piperidine and the naphthalene, could be deduced from this approach (Fig. 4C). Only minor modifications on the 2,4-dimethoxybenzene, such as hydroxylation or O-ethylation, were tolerated to maintain activity. Longer alkyl chain or different simple modifications led to a loss of activity. Changes on the two piperidine moieties and the length of linker between these two also led to a loss of activity. In contrast, the naphthalene moiety could be easily modified without any major loss of activity. A benzene ring with variable groups, for instance, could be introduced. Halogen or alkyl groups attached on this benzene even led to increase activity. The activity was in general increased when lipophilic groups were introduced at this position. The introduction of basicity, as with a pyridine moiety, was on the other hand not tolerated. These results point to the importance of the 2,4-dimethoxybenzene and piperidine moieties for activity of this compound and highlight its specificity. The possibility to modify the naphthalene group opens the way to further optimization of compound B.

Compounds specifically target the Tfp assembly ATPase PilF but not the disassembly ATPase PilT

Tfp are dynamic organelles that constantly undergo cycles of growth, reaching up to several microns in length, and retraction at speeds up to one micron per second (17), and eventually leading to their complete disappearance. This dynamic behaviour is due to the assembly of the major pilin PilE, located into the bacterial inner membrane, into a helical fibre during growth and disassembly of this homopolymer upon retraction. This whole process is made possible by a complex machinery composed of over 15 proteins that spans the inner membrane, the periplasm and the outer membrane. In search for the molecular mechanism responsible for the decrease in piliation that we observed upon bacterial treatment with the compounds, we tested whether pilus retraction was required to induce bacterial disaggregation upon compound treatment. We evaluated the effects of the three compounds on the *pilT* mutant which is unable to retract its pili

and found that preformed *pilT* aggregates were not dissociated upon treatment with the compounds A, B or C and only the formation of new aggregates during the incubation period was inhibited (Fig. 5A, to be compared with Fig. 3E) showing that Tfp retraction is necessary to allow the compounds to carry out their inhibitory effect.

Because these results pointed to an effect of the compounds on Tfp assembly, we turned our attention to the PilF ATPase which generates the energy for the incorporation of pilin monomers in the fibres. Molecular docking of compound B onto the crystal structure of a meningococcal PilF homolog (PDB: 5TSG) indicated eight, sometimes overlapping, potential binding sites with binding energy lower than -7.0 kcal/mol (SI Appendix Fig. S2A). Focusing on four of these sites, five point mutations potentially altering compound B interaction were introduced in the bacteria (SI Appendix Fig. S2B) and the generated strains tested for aggregation to quantify the functionality of their pili (SI Appendix Fig. S2C). Two mutations led to an absence of aggregation likely reflecting a perturbation of PilF enzymatic activity and the absence of pili at the surface of these mutant strains (K371E and D207R; SI Appendix Fig. S2C). Interestingly, R457D and K371A mutations led to normal basal aggregation but to an increase in resistance and sensitivity to compound B, respectively (SI Appendix Fig. S2D). Changes of sensitivity of bacteria to compound B due to single point mutations in PilF support the idea that this enzyme is the target of compound B.

We thus set out to characterize PilF recombinant proteins *in vitro* to evaluate the effect of the compounds on its activity. The full-length *N. meningitidis* PilF recombinant protein was unstable in solution and prone to precipitation at high concentration during purification steps. To circumvent this problem, we produced a truncated form of PilF by deleting the first 165 amino acids encompassing the first N-terminal domain (N1D) and a flexible inter-domain linker (Fig. 5B). Indeed, the N1D-truncated PilF encompassing the second N-terminal domain to the C-terminal end (N2D-CTD), referred to as PilF₁₆₆, remained stable during all purification steps and formed a 254 kDa hexamer as indicated by SEC-MALS (size exclusion chromatography coupled to multi-angle light scattering) and AUC (analytical ultra-centrifugation) (Fig. 5C). Most importantly, the

purified enzyme was highly active in an ATPase activity assay ($K_m = 0.45 \pm 0.05$ mM ; $V_{max} = 25,074 \pm 2,482$ pmol/min/mg, Fig. 5D).

We next investigated whether the ATPase activity of PilF could be inhibited by compounds A-C. At a ratio of 1: 200, the three compounds showed clear inhibitory effects on PilF₁₆₆, bringing its activity down to $44.2 \pm 4.2\%$, $64.8 \pm 3.1\%$, and $29.7 \pm 3.6\%$, respectively (Fig. 5E). A dose response curve indicated that compound B, which showed the most potent inhibitory effect on meningococcal aggregation, has a relative IC₅₀ of 175.10 ± 13.08 μ M on PilF₁₆₆ (protein concentration 1 μ M, Fig. 5F). This value is dependent on the conditions used in the solution-based enzymatic assay and cannot not be easily compared with the IC₅₀ obtained for whole bacteria.

To test whether the same compounds have any effect on the type IV pilus disassembly ATPase PilT, we purified the full-length enzyme and characterized its activity. PilT also readily forms a stable hexamer in solution and exhibited a high ATPase activity (K_m of 0.10 ± 0.02 mM and a V_{max} of $14,232 \pm 664$ pmol/min/mg). Consistently with the results from the aggregation assay, none of the compounds showed any effect on PilT activity (Fig. 5G). The striking inhibitory effects of compounds A, B and C on PilF but not PilT indicate that they target the Tfp assembly but not disassembly process (SI Appendix Fig. S3).

Discussion

In this study, we used a high-throughput microscopy-based screening approach to identify novel compounds preventing the formation of microcolonies on the surface of endothelial cells. We choose this phenotypic approach because it has the potential to reveal active compounds while remaining agnostic on the potential targets involved in bacterial adhesion. Converging with previous studies identifying the role of meningococcal Tfp in the interaction with endothelial cells (11, 13), we discovered compounds that inhibit type IV pili assembly. Because of the importance of this virulence factor *in vivo* (13), these compounds represent attractive candidates for adjuvant therapy in combination with existing antibiotics. Compounds targeting the biogenesis pathways and/or actively blocking the function of large surface machineries involved in the virulence of various bacterial human pathogens have been recently described (10, 18, 19). Various secretion systems have been targeted as well as pilus structures. Certain compounds inhibit the biogenesis of curli pili expressed by *E. coli*, thus reducing biofilm formation (20). Type I pilus biogenesis inhibitors, termed pilicides, have been described to block enteropathogenic or uropathogenic *E. coli* adhesion to host cells and biofilm formation (10). Interestingly, while an *in-silico* study has considered the possibility to inhibit PilF to target type IV pili, no experimental follow up was provided (21). Our study thus describes, for the first time, compounds that directly target type IV pilus biogenesis. At the molecular level, these compounds have a high specificity for the PilF ATPase that powers type IV pilus assembly as they do not affect the activity of the closely related PilT ATPase. This is striking as PilF and PilT are structural homologs of the same AAA+ ATPase family sharing a sequence identity of 30% and they likely act at the same site in the piliation machinery. While compounds A and C are described to target human ATPases (a cyclin dependent kinase and an Akt kinase, respectively), a potential cause of undesirable effects, the structure of compound B, which is the most active, does not match to any known compounds described as a human kinase inhibitor. Accordingly, at efficient concentrations this compound

shows little toxicity on host cells in culture or on the bacteria themselves. Although further studies will need to be undertaken to demonstrate the absence of effects of compound B on cellular proteins, limited side effects are expected. Furthermore, the structure activity relationship performed in this study opens the way to the drug design of novel compounds optimized for *in vivo* administration in terms of solubility and metabolic stability. Certain parts of the compound, in particular the naphthalene group, can be modified without affecting its efficiency and this can be used to make the molecule more soluble and stable. In a more general sense, the identification of PilF as a drugable target also opens new perspectives to the identification of inhibitors affecting not only bacterial adhesion but also pilus-associated virulence functions. Contrary to *in vitro* or *in silico* identification of PilF enzymatic activity inhibitors, this study delivered compounds that are already efficient on whole bacteria.

Beyond the identification of compounds of medical interest this study provides potent tools to further investigate the basic functions of the type IV pilus machinery. Recent cryo-electron microscopy images of Tfp machineries in *Myxococcus xanthus* revealed that the ATPases are located at the base of the machinery on the cytoplasmic side of the inner membrane (22) and further refined the molecular basis for cycles of pilus assembly and disassembly (SI Appendix Fig. S3). PilF and PilT ATPases are thought to alternate at this site, determining the switch between pilus assembly and disassembly. However, potential cues leading to this switch are unknown. Results from our study indicate that the inhibition of PilF activity does not prevent PilT from exerting its activity. Inactive PilF can thus detach from the machinery and be replaced by active PilT. A particular characteristic of the compounds described here is that their effects on piliation rely on the PilT-mediated disassembly of previously formed Tfp. By inhibiting pilus assembly, the inhibitors trigger an unbalanced situation where the retraction of the existing pili leads to their disappearance from the bacterial surface. In absence of PilT the inhibitors of PilF block the further growth of pili but they do not retract, the situation is blocked at a standstill with steady state

amounts of pili. Those compounds will thus be efficient molecular tools to decipher the multiple steps involved in the assembly and disassembly of type IV pili.

Tfp are multifunctional organelles that constitute a particularly appealing therapeutic target. Type IV pili not only allow adhesion to human host cells but also support bacterial auto-aggregation, twitching motility and natural transformation (23). Since the compounds decrease the amount of Tfp, all the associated functions are likely to be affected. Accordingly, in this study we show that bacterial auto-aggregation is affected in addition to adhesion. Further studies will be necessary to test the effect on DNA transformation and twitching motility, two processes also linked to virulence through genetic variation and dissemination on surfaces, respectively. Targeting the surface expression of these organelles is thus a way to affect several virulence-associated properties with the same compound. In addition, beyond *Neisseria meningitidis*, many bacterial species including human pathogens express Tfp (24). The fact that *Neisseria gonorrhoeae* is also sensitive to compound B suggests that such inhibitors could have a broad application. Considering the high degree of conservation among the PilF orthologs, derivatives of those compounds could very well affect additional piliation machineries with an even larger spectrum of effects, as other bacterial systems have similar structures and function in a similar way (24). This is the case of type II secretion systems which are also involved in pathogenesis via secretion of toxins for instance (25). The results reported here have a broad range of applications by opening a way to affect different virulence properties of a large number of pathogens.

This study thus provides, for the first time, compounds active in a *Neisseria meningitidis* adhesion model, through the inhibition of pilus biogenesis. In addition, by identifying the PilF ATPase as a new therapeutic drugable target, these results provide a framework that can be applied to further optimize the obtained compounds and discover new ones. Pharmacokinetic and pharmacodynamic studies will be required in particular to validate the efficiency of these

343 compounds *in vivo* and evaluate the therapeutic window of such pili inhibitors in the course of
344 human pathogenesis.

Materials and Methods

Bacterial strains and growth conditions. *N. meningitidis* 8013 clone 12 used in this study is a serogroup C clinical isolate, expressing a class I SB pilin, Opa2, Opc2, PilC1⁺/PilC2⁺ (26). *N. meningitidis* was grown over-night on GCB agar plates (Difco, France) containing Kellogg's supplements (27) and antibiotics when required. For details, see SI Materials and Methods.

Cell culture. Human umbilical vein endothelial cells (HUVECs; PromoCell) were used between passages 1 and 8 and grown in endothelial serum-free medium (Endo-SFM; Gibco) supplemented with 10% heat-inactivated fetal bovine serum (PAA Laboratories GmbH) and 40 µg/ml of endothelial cell growth supplement (Sigma-Aldrich). For details, see SI Materials and Methods.

Screening method. The SPAI (Signaling Pathways Activators and Inhibitors) library used here is a Sanofi designed collection of 2,239 small compounds having a known target or mechanism of action. HUVEC cells were seeded at a density of 5,000 cells per well in a collagen-coated black 384-well plate with flat transparent bottom and infected at an MOI of 100 bacteria per cell. 384-well plates were then imaged using an Arrayscan automated microscope to visualize bacteria and cell nuclei. For details, see SI Materials and Methods.

Acknowledgments

The authors would like to thank Arthur Charles-Orszag for critical reading of the manuscript. This work was supported by an RPIB grant from the *Agence Nationale pour la Recherche* (ANR); the Integrative Biology of Emerging Infectious Diseases (IBEID) laboratory of excellence and by the VIP European Research Council consolidator grant.

368 DO was supported by a Pasteur-Roux postdoctoral fellowship from the Institut Pasteur.

369

370 **Conflict of interests**

371 The authors declare no conflict of interests.

References

1. van Deuren M, Brandtzaeg P, & van der Meer JW (2000) Update on meningococcal disease with emphasis on pathogenesis and clinical management. *Clin Microbiol Rev* 13(1):144-166, table of contents.
2. Caugant DA & Maiden MC (2009) Meningococcal carriage and disease--population biology and evolution. *Vaccine* 27 Suppl 2:B64-70.
3. Caugant DA, Tzanakaki G, & Kriz P (2007) Lessons from meningococcal carriage studies. *FEMS Microbiol Rev* 31(1):52-63.
4. Toneatto D, Pizza M, Masignani V, & Rappuoli R (2017) Emerging experience with meningococcal serogroup B protein vaccines. *Expert Rev Vaccines* 16(5):433-451.
5. LaForce FM, Djingarey M, Viviani S, & Preziosi MP (2017) Successful African introduction of a new Group A meningococcal conjugate vaccine: Future challenges and next steps. *Hum Vaccin Immunother*:1-5.
6. Rotman E & Seifert HS (2014) The genetics of *Neisseria* species. *Annu Rev Genet* 48:405-431.
7. Finne J, Leinonen M, & Makela PH (1983) Antigenic similarities between brain components and bacteria causing meningitis. Implications for vaccine development and pathogenesis. *Lancet* 2(8346):355-357.
8. Giuliani MM, *et al.* (2006) A universal vaccine for serogroup B meningococcus. *Proc Natl Acad Sci U S A* 103(29):10834-10839.
9. Parikh SR, *et al.* (2016) Effectiveness and impact of a reduced infant schedule of 4CMenB vaccine against group B meningococcal disease in England: a national observational cohort study. *Lancet* 388(10061):2775-2782.
10. Steadman D, Lo A, Waksman G, & Remaut H (2014) Bacterial surface appendages as targets for novel antibacterial therapeutics. *Future Microbiol* 9(7):887-900.
11. Hung MC & Christodoulides M (2013) The biology of *Neisseria* adhesins. *Biology (Basel)* 2(3):1054-1109.
12. DeVoe IW & Gilchrist JE (1975) Pili on meningococci from primary cultures of nasopharyngeal carriers and cerebrospinal fluid of patients with acute disease. *J Exp Med* 141(2):297-305.
13. Melican K, Michea Veloso P, Martin T, Bruneval P, & Dumenil G (2013) Adhesion of *Neisseria meningitidis* to dermal vessels leads to local vascular damage and purpura in a humanized mouse model. *PLoS Pathog* 9(1):e1003139.
14. Bonazzi D, *et al.* (2018) Intermittent Pili-Mediated Forces Fluidize *Neisseria meningitidis* Aggregates Promoting Vascular Colonization. *Cell* 174(1):143-155 e116.
15. Carbonnelle E, *et al.* (2009) Meningococcal interactions with the host. *Vaccine* 27 Suppl 2:B78-89.
16. Imhaus AF & Dumenil G (2014) The number of *Neisseria meningitidis* type IV pili determines host cell interaction. *EMBO J* 33(16):1767-1783.
17. Merz AJ, So M, & Sheetz MP (2000) Pilus retraction powers bacterial twitching motility. *Nature* 407(6800):98-102.
18. Pinkner JS, *et al.* (2006) Rationally designed small compounds inhibit pilus biogenesis in uropathogenic bacteria. *Proc Natl Acad Sci U S A* 103(47):17897-17902.

- 417 19. Lo AW, *et al.* (2014) Suppression of type 1 pilus assembly in uropathogenic
418 Escherichia coli by chemical inhibition of subunit polymerization. *J Antimicrob*
419 *Chemother* 69(4):1017-1026.
- 420 20. Cegelski L, *et al.* (2009) Small-molecule inhibitors target Escherichia coli amyloid
421 biogenesis and biofilm formation. *Nat Chem Biol* 5(12):913-919.
- 422 21. Mehta AS, Snigdha K, Potukuchi MS, & Tsonis PA (2015) Comparative sequence-
423 and structure-inspired drug design for PilF protein of Neisseria meningitidis. *Hum*
424 *Genomics* 9:5.
- 425 22. Chang YW, *et al.* (2016) Architecture of the type IVa pilus machine. *Science*
426 351(6278):aad2001.
- 427 23. Berry JL & Pelicic V (2015) Exceptionally widespread nanomachines composed of
428 type IV pilins: the prokaryotic Swiss Army knives. *FEMS Microbiol Rev* 39(1):134-
429 154.
- 430 24. Giltner CL, Nguyen Y, & Burrows LL (2012) Type IV pilin proteins: versatile
431 molecular modules. *Microbiol Mol Biol Rev* 76(4):740-772.
- 432 25. Cianciotto NP & White RC (2017) Expanding Role of Type II Secretion in Bacterial
433 Pathogenesis and Beyond. *Infect Immun* 85(5).
- 434 26. Nassif X, *et al.* (1993) Antigenic variation of pilin regulates adhesion of Neisseria
435 meningitidis to human epithelial cells. *Mol Microbiol* 8(4):719-725.
- 436 27. Kellogg DS, Jr., Cohen IR, Norins LC, Schroeter AL, & Reising G (1968) Neisseria
437 gonorrhoeae. II. Colonial variation and pathogenicity during 35 months in vitro. *J*
438 *Bacteriol* 96(3):596-605.
- 439

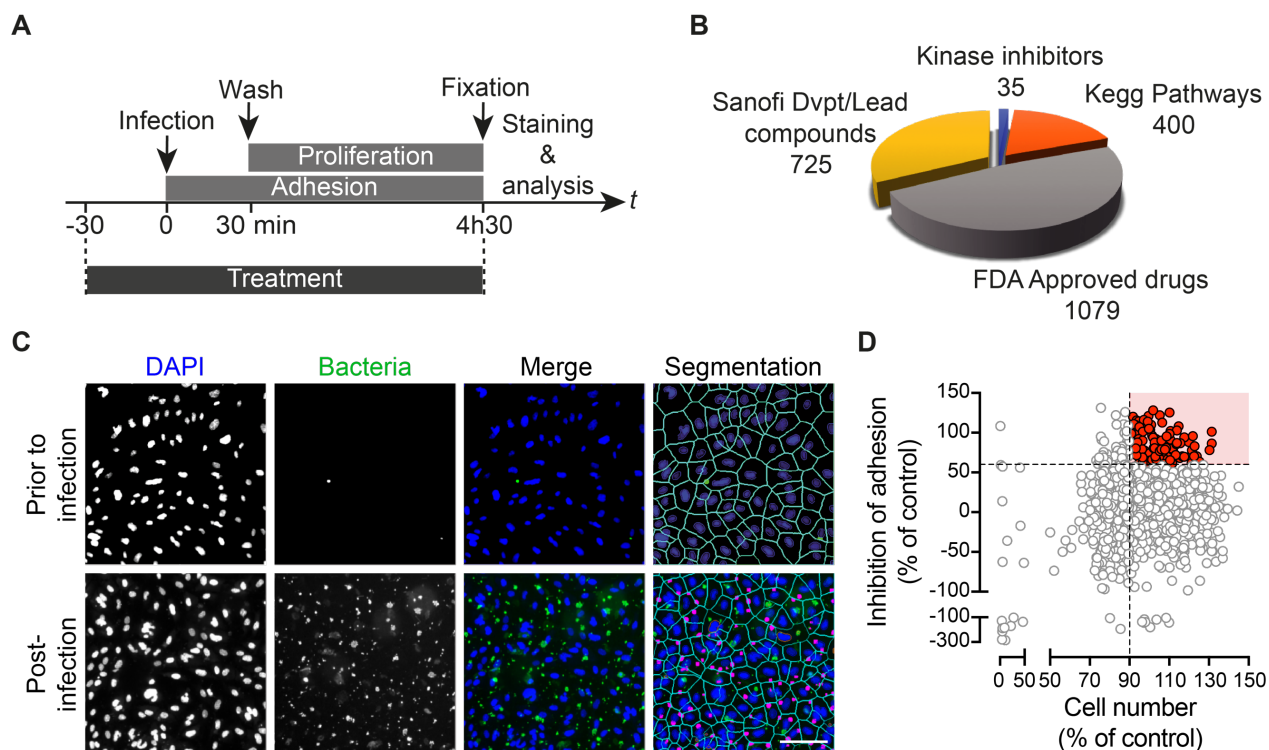


Fig. 1: A high-throughput screening to discover new compounds inhibiting *N. meningitidis* adhesion to human endothelial cells. (A) Timeline of the infection and treatment protocol used in the screen. **(B)** Description of the library used in the screen. **(C)** Image analysis readout of the screen. Scale bar, 100 μ m. **(D)** XY plot showing the 163 compounds considered for further analysis (red dots) among the total of the 2,239 tested compounds. The horizontal and vertical dashed lines represent the thresholds used to select the hit compounds (inhibition of bacterial adhesion $\geq 60\%$ and cellular toxicity $\leq 10\%$, respectively). Data are representative of N=2 independent experiments.

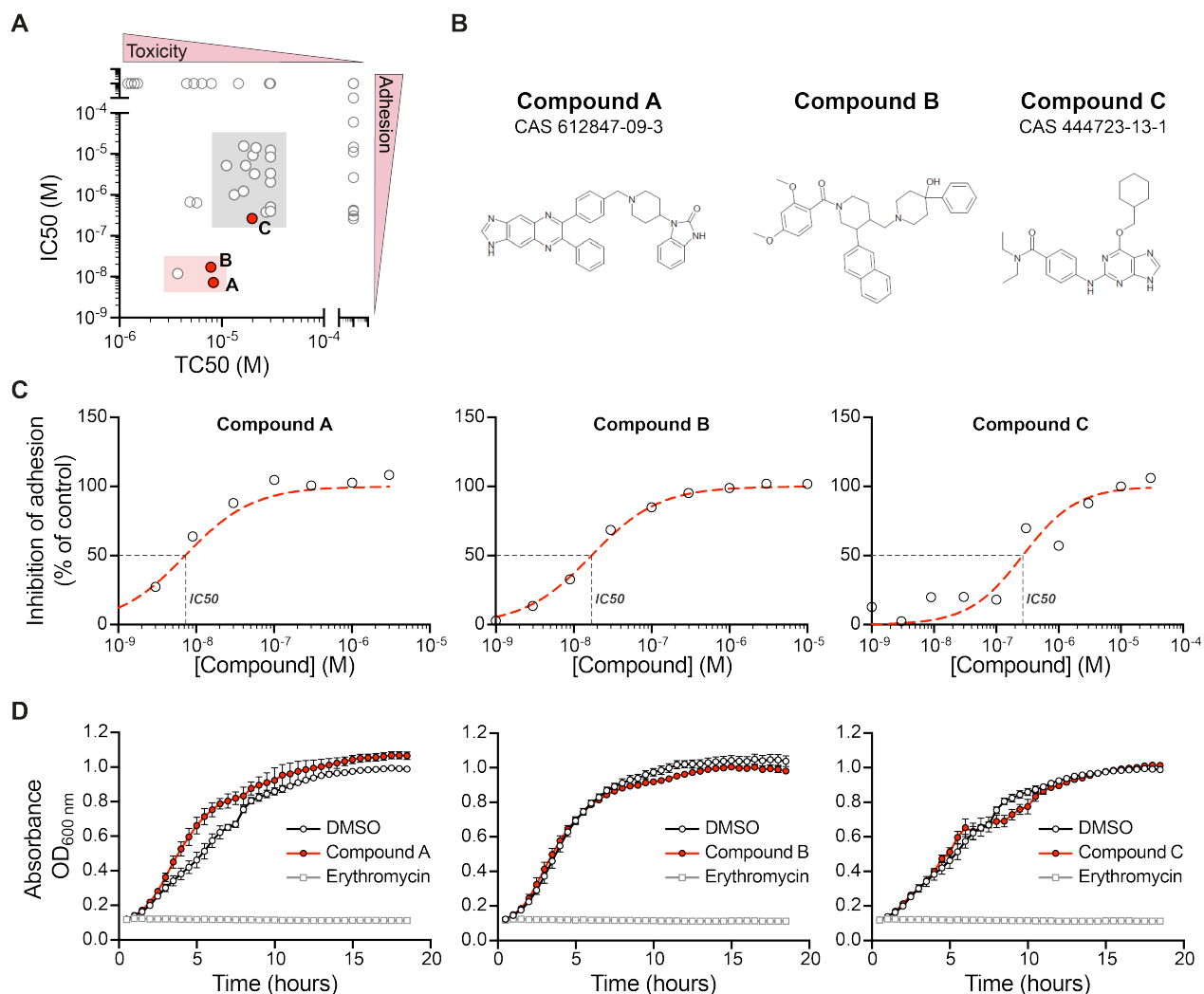


Fig. 2: Identification of hit compounds affecting bacterial adhesion but not bacterial viability. (A) XY plot showing the IC₅₀ of adhesion to HUVEC cells and TC₅₀ values of each of the 59 tested compounds on HepG2 cells. Red dots highlight the 3 compounds chosen for further characterization and referred to as A, B and C, hereafter. (B) Chemical structure of the selected hits with their identification number. (C) Dose response curves of the efficiency of the 3 hit compounds in inhibiting bacterial adhesion. The red dashed lines show the non-linear fit used to determine the IC₅₀. (D) Growth curves of *N. meningitidis* in the presence of either DMSO as vehicle control, 1 μ M of the indicated hit compound or 3 μ g/ml of Erythromycin as negative growth control. Data represent the mean \pm SEM of N=3 independent experiments, each performed in duplicate.

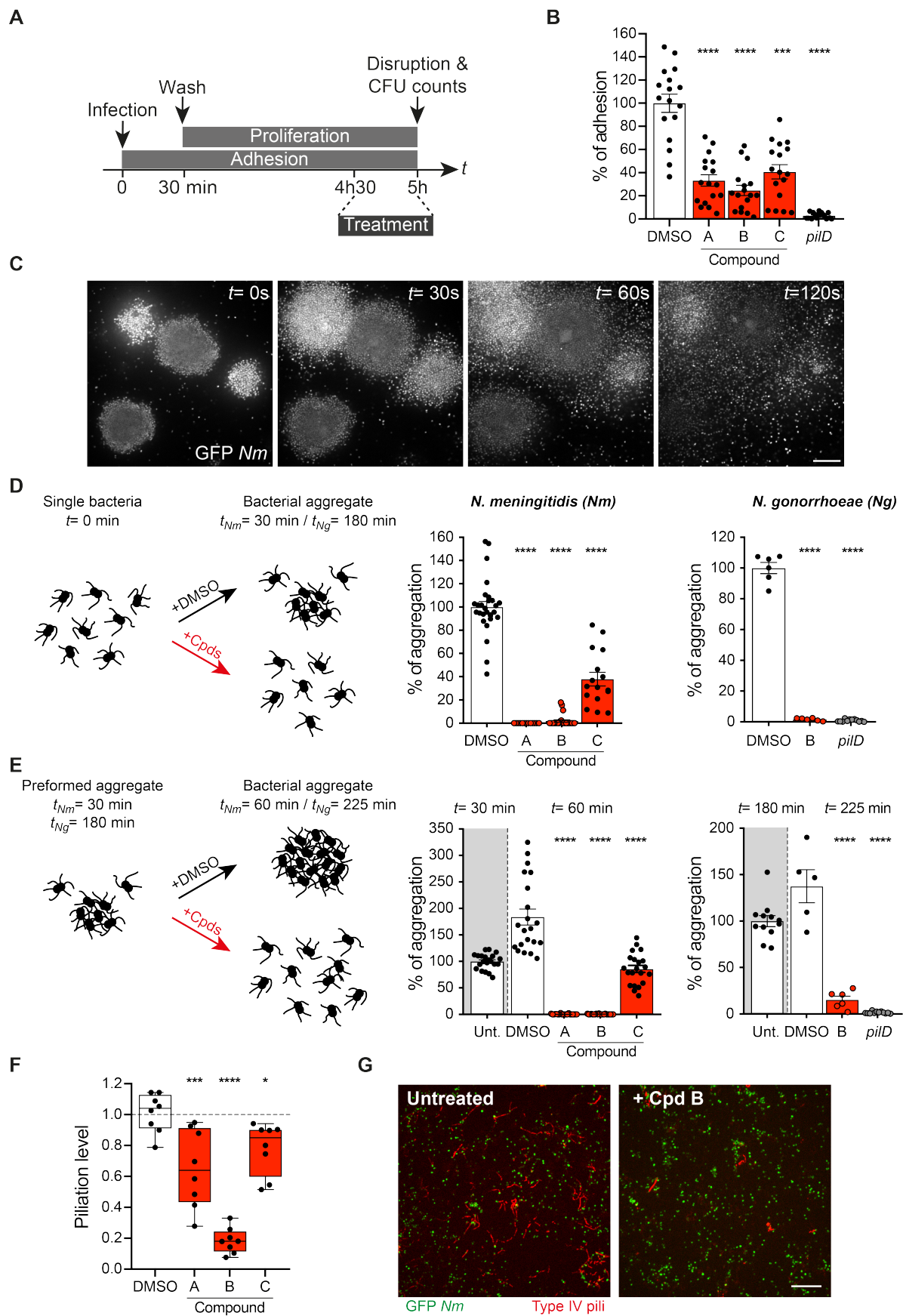


Fig. 3: Compounds efficiently inhibit bacterial aggregation by decreasing their level of piliation. **(A)** Timeline of the infection and treatment protocol used to test the ability of the 3 compounds to detach previously adhering bacteria. **(B)** Quantification of the ability of the compounds to detach adhering bacterial microcolonies as measured by colony forming units (CFU) counts. DMSO, in which compounds are dissolved, is used as a control. The non-piliated and thus non-adhesive *pilD* mutant is used as a negative control. Data were normalized with respect to the mean value of the control condition per replicate. Data represent the mean \pm SEM of N=6 independent experiments, each performed in triplicate. **(C)** Pre-formed aggregates of GFP-expressing *N. meningitidis* were treated with 1 μ M of compound B while being observed by time-lapse video fluorescence microscopy. Scale bar, 20 μ m. **(D-E)** Description and quantification of the impact of treatment (1 μ M) on the ability **(D)** of the bacteria to form aggregates or **(E)** to induce the disaggregation of preformed aggregates in both *N. meningitidis* (left) and *N. gonorrhoeae* (right). Data represent the mean \pm SEM of N=6 and N=3 independent experiments for *N. meningitidis* and *N. gonorrhoeae*, respectively, each performed in triplicate. **(F)** Effect of the hit compounds on the surface expression of bacterial Tfp. Each dot represents an independent experiment performed in triplicate. Data represent quartiles in box and whiskers format. **(G)** Visualization by fluorescent microscopy of bacterial Tfp surface expression. GFP-expressing bacteria appear as green dots while pili labelled with a monoclonal antibody appear as red filaments. Scale bar, 20 μ m. Treatment with compound B (1 μ M) is compared to an untreated sample. A one-way ANOVA test comparing with the DMSO condition was used to determine statistical significance. * $P \leq 0.05$; ** $P \leq 0.01$; *** $P \leq 0.001$; **** $P \leq 0.0001$.

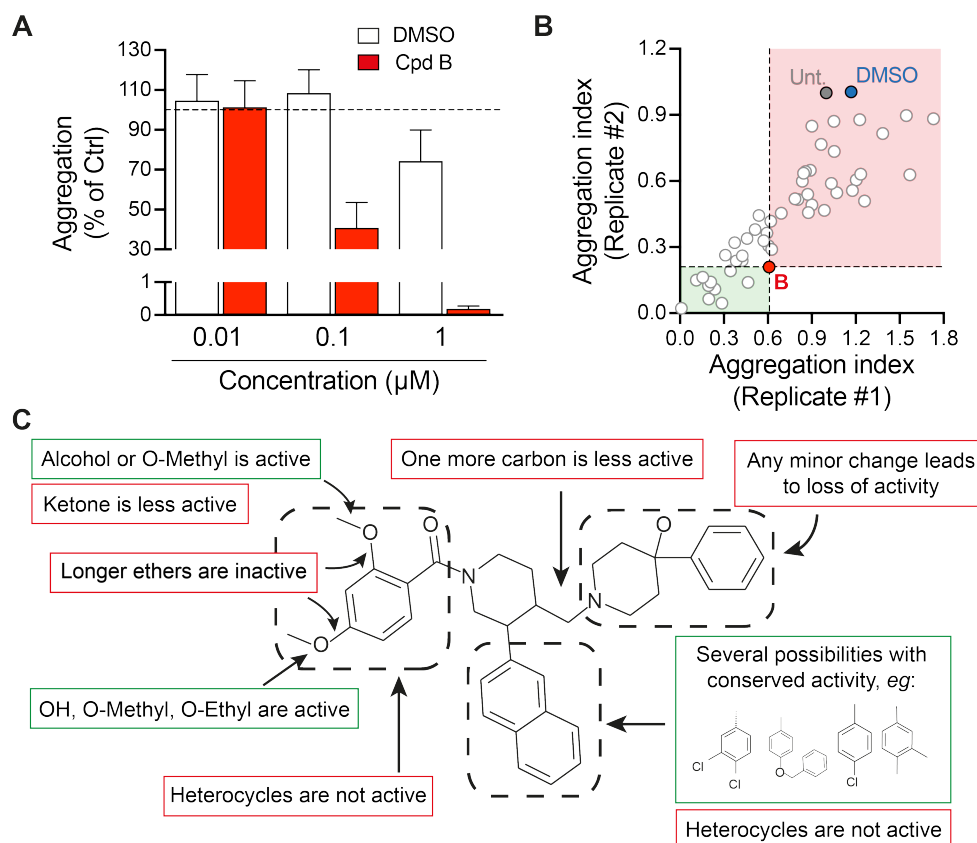


Fig. 4: Structure activity relationship of compound B. **(A)** Quantification of the impact of indicated concentration of compound B on the ability of the bacteria to form aggregates. Data represent the mean \pm SEM of N=2 independent experiments, each performed in triplicate. **(B)** Quantification of the impact of the 49 derivatives of compound B on the ability of bacteria to form aggregates. Data were normalized with respect to the untreated condition in each replicate. The aggregation indexes of compound B in each of the two replicates were used as thresholds to determine derivative compounds with a better (light green) or a worst (light red) activity than compound B (red dot). **(C)** Molecular activity map of compound B.

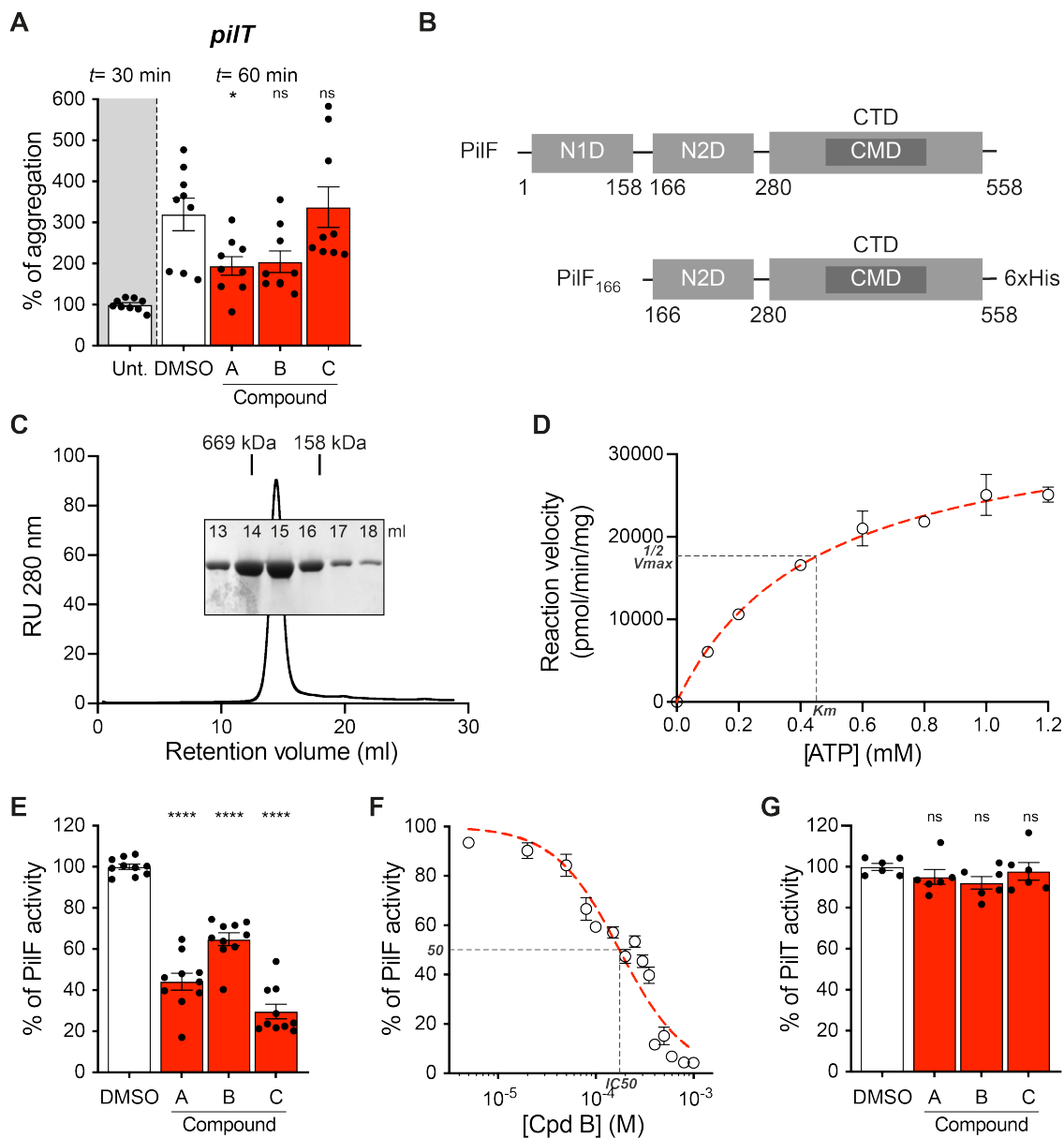


Fig. 5: Compounds specifically target the Tfp assembly PilF ATPase. (A) Effect of the hit compounds on the disaggregation of pre-assembled bacterial aggregates formed by the *pilT* mutant. Data represent the mean \pm SEM of N=3 independent experiments, each performed in triplicate. Data were normalized with respect to the mean value of the untreated condition (t=30min) per replicate. **(B)** Schematic illustration of *N. meningitidis* full-length and truncated PilF. N1D, N-terminal domain 1; N2D, N-terminal domain 2; CTD, C-terminal domain; CMD, coordinated metal domain. **(C)** Size exclusion profile of *N. meningitidis* PilF₁₆₆ on a Superose 6

column. SDS-PAGE followed by Coomassie staining shows the peak fraction of PilF₁₆₆ hexamer. Elution volumes of aldolase (158 kDa) and thyroglobulin (669 kDa) are indicated. **(D)** Reaction velocity of PilF in function of the ATP concentration in an ATPase activity assay. The Michaelis constant K_m is determined as the concentration value corresponding to half of the maximum velocity (V_{max}). **(E)** Effect of the hit compounds on the activity of PilF₁₆₆. 1 μ M of PilF₁₆₆ protein was incubated with 200 μ M of indicated compound. Data represent mean \pm SEM of N=5 independent experiments, each performed in duplicate. Results were normalized with respect to the mean value of the DMSO control condition per replicate. **(F)** Dose response curve of compound B on the activity of PilF₁₆₆. 1 μ M of PilF₁₆₆ protein was incubated with various amounts of compound B and ATPase activity was measured. Results are indicated as the percentage of the untreated sample. **(G)** Effect of the hit compounds on the activity of the PilT ATPase. 1 μ M of PilT protein was incubated with 200 μ M of indicated compound. Data represent mean \pm SEM of N=3 independent experiments, each performed in duplicate. Results were normalized with respect to the mean value of the DMSO control condition per replicate. A one-way ANOVA test comparing with the DMSO condition was used to determine statistical significance. ns, non-significant; * $P \leq 0.05$; **** $P \leq 0.0001$.

Supplementary Materials and Methods

Bacterial strains and growth conditions. *N. meningitidis* 8013 clone 12 used in this study is a serogroup C clinical isolate, expressing a class I SB pilin, Opa2, Opc2, PilC1⁺/PilC2⁺ (1). *N. meningitidis* was grown over-night on GCB agar plates (Difco, France) containing Kellogg's supplements (2) and antibiotics when required: 2 µg/ml erythromycin (*pilF*_{ind}), 50 µg/ml spectinomycin (Δ *pilF*) or chloramphenicol 5 µg/ml (GFP-expressing strains). For liquid cultures, bacteria were adjusted to an OD_{600nm} of 0.05 in GCB broth with Kellogg's supplement (3). *N. gonorrhoeae* MS11 was grown over-night on Chocolat + PolyVitex agar plates (bioMérieux) containing antibiotics when required: 2 µg/ml erythromycin (GFP-expressing strains) or 100 µg/ml kanamycin (Δ *pilD*). For liquid cultures, bacteria were adjusted to an OD_{600nm} of 0.1 in GCB broth with Kellogg's supplement (4). All cultures were incubated at 37°C under moist atmosphere containing 5% CO₂ (3, 4). *Escherichia coli* XL1-Blue, used to generate the *pilF* mutant strains of *N. meningitidis*, was grown at 37°C on liquid or solid Luria-Bertani medium (Difco) containing 50 µg/ml kanamycin.

Cell culture. Human umbilical vein endothelial cells (HUVECs; PromoCell) were used between passages 1 and 8 and grown in endothelial serum-free medium (Endo-SFM; Gibco) supplemented with 10% heat-inactivated fetal bovine serum (PAA Laboratories GmbH) and 40 µg/ml of endothelial cell growth supplement (Sigma-Aldrich) or in EBM-2 endothelium basal medium (Lonza) supplemented with EGM-2 endothelium medium kit (Lonza) and 10% decompartmented fetal calf serum.

Screening method. *Screening library.* The SPAI (Signaling Pathways Activators and Inhibitors) library is a Sanofi designed collection of 2,239 small compounds having a known target or mechanism of action and therefore serves as a pharmacological toolbox to probe phenotypes in disease relevant cellular models. This library includes: 1,079 small molecules that are FDA approved drugs (including 207 human targets and main classes of antibiotics), 400 compounds are known reference inhibitors of cellular and metabolic pathways, 725 compounds are Sanofi lead molecules discovered in previous screening projects, which are potent modulators of cellular pathways and 35 compounds are known kinase inhibitors. The detailed composition of this library is proprietary to Sanofi and screening hit structures and properties have been disclosed to the team after a clearance check-up where no conflict of interest has been identified with other internal projects.

Adhesion assay screening. *Neisseria meningitidis* were seeded a day before the screening on tryptic soy agar gelose from a stock conserved at -80°. On the screening day, a colony was picked for

dilution in 12 ml of culture medium and adjusted to an optical density at 600 nm (OD_{600nm}) of 0.16 for subsequent growth under agitation for 3 hours. The CFUs were evaluated by optical density and comparison to a reference growth curve and diluted in order to provide a MOI of 100 bacteria per cell, hence 500,000 CFUs per 5 µl solution to be added to each well.

HUVEC cells were seeded at a density of 5,000 cells per well in a collagen-coated black 384-well plate with flat transparent bottom and incubated for 24 hours. Culture medium was replaced with culture medium supplemented with 20 µg/ml Hoechst 33432, test compounds prepared in DMSO were added with a Bravo 384 wells Agilent dispenser (0.5 µl per well for a final concentration of 10 µM compound and 1% DMSO) and cells were incubated for 30 minutes. After 2 washes with a Tecan Hydrospeed washer, fresh culture medium containing the same compound concentrations was added at the lowest speed using a multidrop dispenser.

Bacteria in exponential phase from the 3-hour liquid culture were added in a 5 µl volume using a multidrop dispenser. Columns 1 and 2 were not seeded with bacteria to serve as a reference for image analysis to evaluate a 100% adhesion inhibition. Columns 3 and 4 were not treated with compounds to serve as a reference for a 0% adhesion inhibition. After a 30-minutes incubation with bacteria, the supernatant was aspirated and replaced with fresh medium containing the same compound concentrations and plates incubated for an additional 4 hours. Culture medium was then aspirated and cells were fixed with formalin for 30 minutes at room temperature. After two washes with PBS, bacteria were stained using a Group C *Neisseria meningitidis* antiserum produced in rabbit (BD Bioscience) and an AlexaFluor488-conjugated goat anti-rabbit secondary antibody (Life Technologies) and host cells were detected with a DNA labelling dye (Hoechst 33342). Plates were then conserved at 4°C until ready to proceed to image acquisition.

Image acquisition and analysis. 384-well plates were imaged using an Arrayscan automated microscope equipped with a BGFR_386_23 filter (Hoechst 33342) and a BGFR_485_20 (AlexaFluor488) (Thermofischer). A minimum of 5 fields of view and 500 nuclei per well were quantified. For each condition, image analysis and segmentation allowed the determination of the mean number of spots (bacteria) per object (cells) (Spot Detector V3 Bioapplication, Thermofischer). The percentage of bacterial adhesion inhibition for each tested compound was then calculated with respect to columns 1-2 and 3-4 representing negative (no bacterium, 0% adhesion) and positive controls (no treatment, 100% adhesion), respectively.

Hit compound selection. The strategy of hit compound selection relied on both the ability of the tested compounds to efficiently inhibit bacterial adhesion but also to display a low cellular toxicity. Therefore, compounds inducing a decrease in the cell number superior at 90% of the control wells were discarded. Finally, were selected as hits, compounds leading to a percentage of adhesion

inhibition superior or equal to 60%.

Dose response assay. A dose response approach with compound concentrations ranging from 1 nM to 30 μ M was used to determine both the half maximal inhibitory concentration (IC₅₀) and the median toxic concentration (TC₅₀) of each selected compound. Briefly, for IC₅₀ calculation, 30 min post-infection of endothelial cells, compounds at the indicated concentrations were added to individual wells for 4 hours and the inhibition of bacterial adhesion was monitored as previously described. The cellular toxicity (TC₅₀) was evaluated on THP1 and HepG2 cells by monitoring their growth inhibition upon 40 hours' exposure to the indicated compound concentrations. Cell viability was assessed based on the quantitation of the ATP present in the culture using the CellTiter-Glo Luminescent Cell Viability Assay (Promega) according to manufacturer instructions.

***Neisseria meningitidis* growth curves.** Bacterial overnight cultures were diluted in Endo-SFM containing 10% fetal bovine serum to an OD_{600nm} of 0.05 and allowed to proliferate until an OD_{600nm} of 0.2. This pre-culture was then diluted to an OD_{600nm} of 0.05 and 150 μ l of the bacterial suspension was transferred into wells of a 96-well plate. Bacteria were then treated with either 1 μ M of the indicated compound, 3 μ g/ml of Erythromycin or DMSO as negative and positive growth controls, respectively, each performed in duplicate. Plates were then placed in a Cytation 5 multimode reader (Biotek) at 37°C with 5% CO₂ and continuous agitation and optical densities at 600 nm were recorded every 30 minutes for 18 hours.

Bacterial detachment assay. 10⁵ HUVECs were plated into wells of 24-well plates and incubated over-night. Monolayers were then infected with 10⁷ bacteria (MOI of 100). After 30 min, unbound bacteria were removed by three washes, and the infection was continued for 4 h. Compounds were then added at a final concentration of 1 μ M and incubated for additional 30 minutes. Finally, after 3 washes, adherent bacteria were recovered by trypsin treatment of the infected cells and bacteria counted by plating appropriate dilutions on GCB agar plates. Results were normalized according to the effective concentration of the bacterial inoculum, which was also determined by CFU counts.

Immunofluorescence on immobilized bacteria. A GFP-expressing bacterial suspension at OD_{600nm} of 0.1 in PBS was placed in a glass-bottom 96-well plate (Greiner), centrifuged for 10 min at 4,000 g. Medium was removed, the remaining film was dried for 10 minutes at 37°C and bacteria were fixed in PBS containing 4% paraformaldehyde for 15 min. After 3 washes, samples were blocked with PBS containing 0.2% gelatine (PBSG) for 20 min. Pili were detected using the 20D9 mouse monoclonal antibody diluted at 2.5 μ g/ml in PBSG followed by a AlexaFluor568-conjugated goat anti-mouse secondary antibody (Life technologies). Mowiol was then added to the wells prior to imaging.

Bacterial aggregation assay. *Neisseria meningitidis*: Bacteria grown over-night on GCB agar

plates were adjusted to an OD_{600nm} of 0.05 and incubated for 2 h at 37°C in RPMI medium supplemented with 10% FBS. The bacterial pre-culture was concentrated to an OD_{600nm} of 0.3 by a centrifugation at 15,000 g for 1 min followed by resuspension in medium containing DAPI (0.1 ng/ml) when required. Bacterial suspensions were briefly vortexed, transferred into wells of a 96-well μ -plate with square wells (Ibidi) and allowed to form aggregates for a period of 30 minutes either in the presence of or prior to the addition of the indicated compound at the indicated concentrations.

N. gonorrhoeae: GFP-expressing bacteria grown over-night on Chocolat + PolyVitex agar plates were adjusted to an OD_{600nm} of 0.1 in GCB broth with Kellogg's supplement, briefly vortexed and 100 μ l were transferred into wells of a 96-well μ -plate with square wells (Ibidi). Bacterial suspension was allowed to form aggregates for a period of 180 minutes, as previously described (5), either in the presence of or prior to the addition of compound B at a final concentration of 1 μ M or DMSO as control for 45 min.

Aggregation analysis: Aggregates/bacteria were then observed under the microscope and four fluorescence images per well were captured using a 4x objective. Size of aggregates and numbers of bacteria involved in aggregates relative to the total amount of bacteria were determined with a homemade script in the ImageJ software (6). Briefly, all the images were initially processed by converting to an 8-bit format. Background was subtracted, and the auto-threshold plug-in was used. Finally, aggregates were identified by particles analysis, their volume calculated and the number of bacteria involved determined allowing the calculation of the percentage of bacteria participating in aggregates relative to the total number of bacteria introduced in the well (7). Data shown were normalized with respect to the mean value of the control condition per replicate.

Statistics. All graphs and statistical analysis were performed with GraphPad Prism 7 (GraphPad Software). No statistical method was used to predetermine sample size. Kolmogorov–Smirnov test was used to assess normality of all data sets. Boxes in box plots extend from the 25th to 75th percentile, with a line at the median and whiskers extend from the 10th to the 90th percentile. Bar graphs show the mean \pm SEM.

Type IV pili quantification by ELISA. Bacteria were resuspended from fresh GCB plates in PBS at OD_{600nm} of 0.1. Serial two-fold dilutions were performed and dispensed within the wells of 96-well plates (Nunc). The plates were centrifuged for 10 min at 3,220 g, and the supernatant was carefully removed. Then, plates were incubated without cover at 37°C for 10 min to allow drying. Bacteria were fixed with a solution of PBS containing 4% paraformaldehyde for 15 min. Coated plates were washed 3 times with PBS and incubated in blocking solution (1X PBS, 1% BSA, 0.1% Tween-20) for 10 min. The 20D9 anti-PilE mouse monoclonal antibody, diluted at a concentration

of 0.25 µg/ml in blocking solution, was added to the plates and incubated for 1 h. After several washes, a peroxidase-conjugated anti-mouse IgG antibody, diluted at 1/10,000 in blocking solution, was added to the wells for 1 h. Finally, after three washes, the staining was revealed using TMB (tetramethylbenzidine) substrate and stop solution following the manufacturer's instructions (BD Bioscience). The absorbance was read at 450 nm using a microtiter plate reader (Flex station 3, Molecular Devices).

Autodocking. Docking was performed using AutoDock Vina (8) and AutoDock Tools 4.2 (9). A homology model of *Neisseria meningitidis* PilF was generated based on the crystal structure of *Geobacter metallireducens* PilB (PDB: 5TSG) using the HHpred server (10). The search was carried out using default parameters in a grid volume encompassing the entire PilF hexamer. The torsional degree of freedom for compound B (the ligand) is set manually based on its chemical properties. The flexibility of PilF (the receptor) is omitted.

Generation of *pilF* point mutations in *N. meningitidis*. Point mutations in the *pilF* gene of *N. meningitidis* were generated using a single-primer one-step mutagenesis process (11). Briefly, a mutagenic primer (listed in the table below where mutated nucleotides are shown in lower case and the corresponding codon in bold red) was used to amplify the pCR2.1*ΩpilF* plasmid (coding for the wild-type sequence of PilF) (7) by PCR using Phusion polymerase. The PCR product was digested using FastDigest DpnI at 37°C for 2 hours and then inactivated at 80°C for 5 minutes to degrade the pCR2.1*ΩpilF_{WT}* plasmid. The resulting product was transformed in XL1-Blue *E. coli*, which were then selected on kanamycin-containing LB plates. Plasmids from single colonies were isolated, sequenced and the mutated fragments were subcloned into the pGCC4 vector under the control of the Lac promoter (*pilF_{ind}*) (12) using PacI and PmeI restriction enzymes. The plasmids were used to transform GFP-expressing *N. meningitidis* (3) and transformants were selected on erythromycin plates. The wild type *pilF* gene was then inactivated as described (7).

Primer	Sequence
PilF-D207R	CGTTTCCGTGTG cgC GGGCAGCTCCGCGAG
PilF-K371E	TTTGCCGCTGCTTTG gAG TCTTTCCTGCGT
PilF-K371A	TTTGCCGCTGCTTTG gcGT TCTTTCCTGCGT
PilF-E390K	GAGATTTCGTGATTTG aAA ACTGCCGATATT
PilF-R457D	AAACAGGAAGTGGA gaC CCGTCTGCCTCT

PilF and PilT purification. *Cloning.* Genomic DNA were extracted from the *N. meningitidis* 8013 strain using a commercial DNA extraction kit (Invitrogen). Various constructs containing different domain organizations of PilF and PilT conjugated to a 6xHis tag were cloned into the pET11a vector. Plasmids with the correct sequences were amplified in *E. Coli* DH5α cells and transformed into *E. Coli* BL21(DE3) competent cells for recombinant protein expression. Small scale

expression tests were performed to determine the best expression temperature, time and induction conditions prior to large scale protein production.

Production. A truncated form of *N. meningitidis* PilF containing the second N-terminal domain and the C-terminal domain (N2D-CTD, residues 166-568), PilF₁₆₆, was used in all *in vitro* assays in this study. PilF₁₆₆-expressing bacteria were inoculated and grown in 1 L of lysogenic broth (LB) Miller containing Ampicilin at 37°C under 180 rpm agitation. The PilF₁₆₆ culture was induced with 0.2 mM IPTG at an OD_{600nm} of 0.6. The cells were then cultured at 18°C under 180 rpm agitation for 18-20 hours. The same protocol was used to induce and express the full-length *N. meningitidis* PilT. Both PilF₁₆₆ and PilT cells were harvested by centrifugation at 4,700 rpm at 4°C for 45 min, washed briefly with PBS and pelleted again at 6,500 rpm, 4°C before being flash frozen with liquid nitrogen and stored at -80°C.

Purification. The deep-frozen pellets were thawed on ice for 30 min under 100 rpm agitation with added lysis buffer (20 mM Hepes pH 8.0, 500 mM NaCl, 10 mM MgCl₂, 5% glycerol, 1 mg/ml lysozyme and 5 units of benzonase). The resuspended cells were sonicated for 10 s with 30 s intervals and 30% amplitude for 15 rounds. The cell lysis was then centrifuged at 11,000 rpm for 1 hour. The supernatant was then loaded onto a 5 ml HP HisTrapTM IMAC column (GE Healthcare Life Sciences). A gradient wash procedure using 50 ml of wash buffer (20 mM Hepes pH 8.0, 500 mM NaCl, 10 mM MgCl₂, 5% glycerol, 0-10 mM imidazole) was performed. The His-tagged proteins were then eluted using elution buffer (20 mM Hepes pH 8.0, 500 mM NaCl, 10 mM MgCl₂, 5% glycerol, 350 mM imidazole). The eluted protein solution was concentrated to 1 mL using an Amicon Ultra-15 centrifugal filter (30 kDa cut-off) at 3,500 rpm, 4°C. The concentrated protein was injected into a Superose 6 10/30 column (GE Healthcare Life Sciences) for size exclusion chromatography (SEC). SEC was performed at 4°C in SEC buffer (20 mM Hepes pH 8.0, 150 mM NaCl, 10 mM MgCl₂). A SDS-page gel analysis was then performed to determine the protein purity of each peak fraction. Fractions containing PilF₁₆₆ or PilT (purity > 98%) were combined and concentrated to around 3 mg/ml. A fraction of the freshly purified proteins was used to perform SEC-MALS and AUC experiments while the remaining amount flash frozen with liquid nitrogen and stored at -80°C.

ATPase activity assay. Purified PilF₁₆₆ or PilT was thawed on ice and centrifuged at 130,000 rpm for 20 min at 4 °C to remove aggregated protein. In a 50 µL reaction volume, 1 µM PilF₁₆₆ or PilT was incubated with 0.1-1.2 mM freshly made ATP at 37 °C in activity buffer (20 mM Hepes pH 8.0, 150 mM NaCl, 5 mM MgCl₂). After an reaction time of 0 min, 20 min, 40 min and 60 min, a malachite green molybdate-based solution was added to measure the inorganic phosphate release, as described (13). The colorimetric reaction was stopped by adding 10 µL 34% citric acid. After

10-min incubation the absorbance at 630 nm was measured at room temperature and calibrated using a free phosphate standard. The activity of PilF₁₆₆ or PilT is represented by enzymatic velocity with unit pmol/min/μg. To extract the kinetic constants K_m and V_{max}, the reaction rate was plotted against ATP.

SDS–PAGE. Preparation of protein samples, SDS–PAGE separation, transfer to membranes, and immunoblotting were performed using standard biochemistry techniques (14). Proteins were separated by SDS–PAGE in Tris-glycine gels containing 12–15% acrylamide.

SEC-MALS. Freshly purified *N. meningitidis* PilF₁₆₆ and PilT was analysed in activity buffer at room temperature using a SEC-MALS (multi-angle light scattering) system in which an analytical Superose 6 10/30 column (GE Healthcare Life Sciences) was coupled to a static light-scattering (DAWN HELEOS II, Wyatt Technology) equipment. An Agilent 1200 UV (Agilent Technologies) detectors was used to capture the UV signal of each elution volume. Data analysis was done using the ASTRA software package (Wyatt Technology).

Analytical ultracentrifugation. AUC sedimentation velocity experiments were conducted in activity buffer at 20°C using a Beckman Optima XL-I analytical ultracentrifuge and an An-60 Ti rotor (Beckman) in absorbance mode (280 nm incident light) at 40,000 rpm rotor speed. A total number of 100 scans were collected with one scan every 6 min. Scans 6–100 were analysed with Sedfit (15) and a c(s)-based sedimentation profile analysis was performed. Expected sedimentation coefficients and molecular weight of the structural models were predicted using PROHYDROUS-SOMO (16).

Supplementary Figures

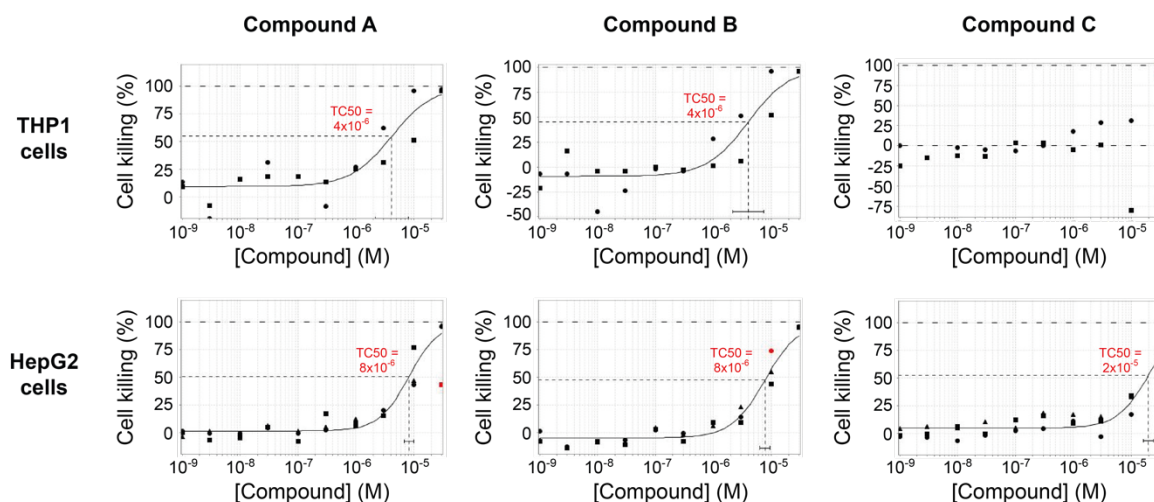


Fig. S1. Absence of cellular toxicity of the selected compounds. THP1 and HepG2 cells were cultured for 40 h at 37°C under moist atmosphere containing 5% CO₂ in presence of the indicated compound concentrations and cell viability was assessed based on the quantitation of the ATP present in the culture using the CellTiter-Glo Luminescent Cell Viability Assay (Promega) according to manufacturer instructions. Results were normalized with respect to the control condition per replicate and expressed as the percentage of cell killing. Dots, squares and triangles in graphs represent technical replicates (N=2 and N=3 independent experiments for THP1 and HepG2, respectively). Red symbols represent outliers excluded for curve fitting and TC50 calculation.

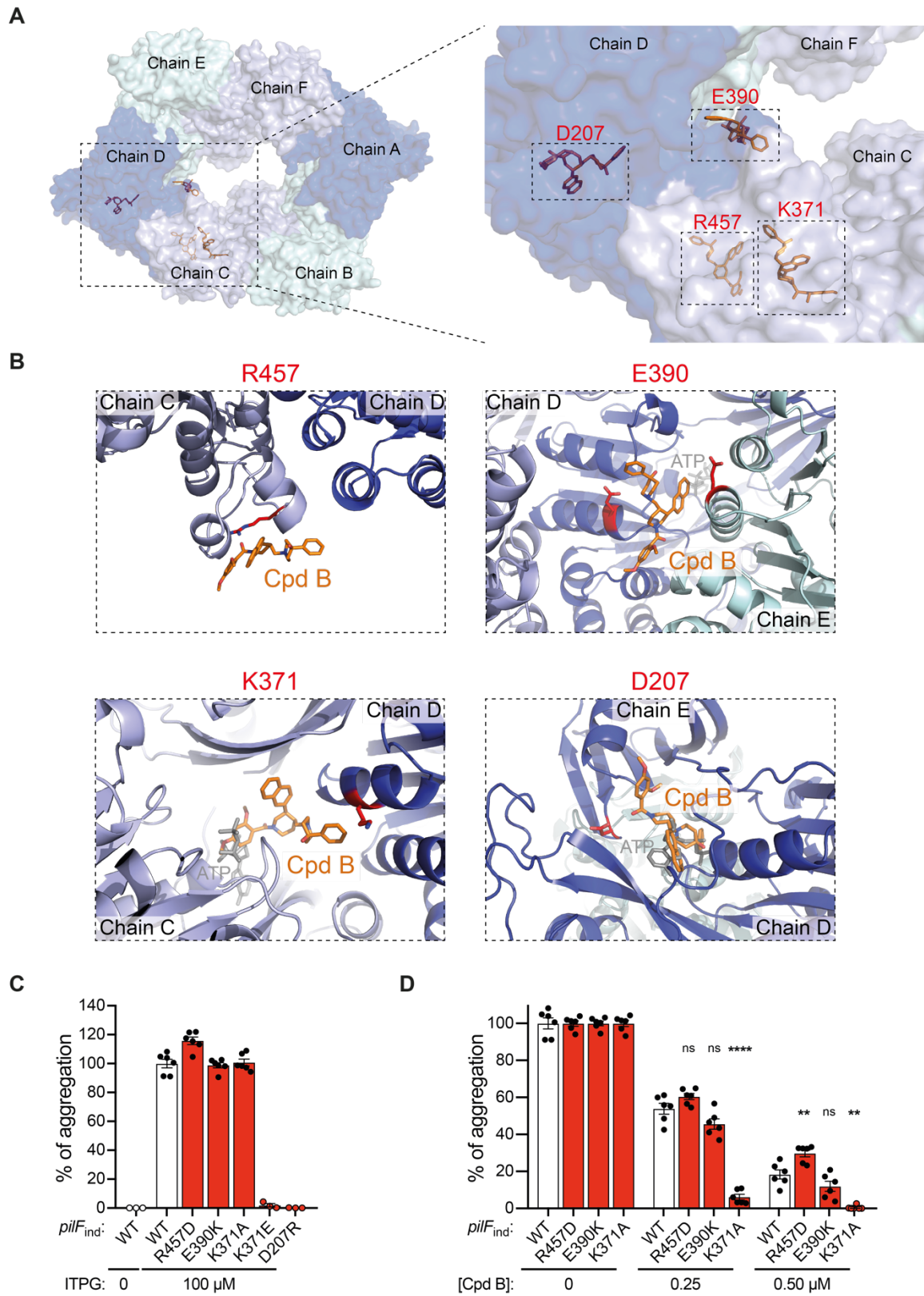


Fig. S2. Point mutations in *Neisseria meningitidis* PilF are sufficient to tune bacterial sensitivity to compound B. (A) *In silico* docking simulations between compound B and the

homology model of *Neisseria meningitidis* PilF. The represented top four docking solutions with a binding energy lower than -7.0 kcal/mol, which occupies four different predicted interaction sites are shown. The PilF hexamer, shown in surface representation (60% transparency), is colored in blue for chain A and D, in cyan for chain B and E, and in light blue for chain C and F, respectively. Compound B is colored in orange. A zoomed-in view is provided on the right. **(B)** Detailed view of the four putative binding sites. Compound B in stick representation is colored in orange. ATP molecule in the putative catalytic pocket is shown in grey. Amino-acids potentially involved in the compound B-PilF interaction and selected for mutagenesis are highlighted in red. **(C)** Aggregative properties of the different PilF mutant strains generated. Data were normalized with respect to the IPTG-induced (100 μ M, 2h) $\Delta pilF pilF_{ind}$ WT strain. **(D)** Effect of compound B on the aggregative property of the IPTG-induced (100 μ M, 2h) $\Delta pilF pilF_{ind}$ mutant stains generated. Data were normalized with respect to the DMSO control condition ([Cpd B]: 0 μ M) per bacterial strain and replicate to minimize the effects of inter-strain variation in absence of drug. **(C-D)** Data represent the mean \pm SEM of N=2 independent experiments, each performed in triplicate. A one-way ANOVA test comparing with the control condition was used to determine statistical significance. ns, non-significant; ** $P \leq 0.01$; **** $P \leq 0.0001$.

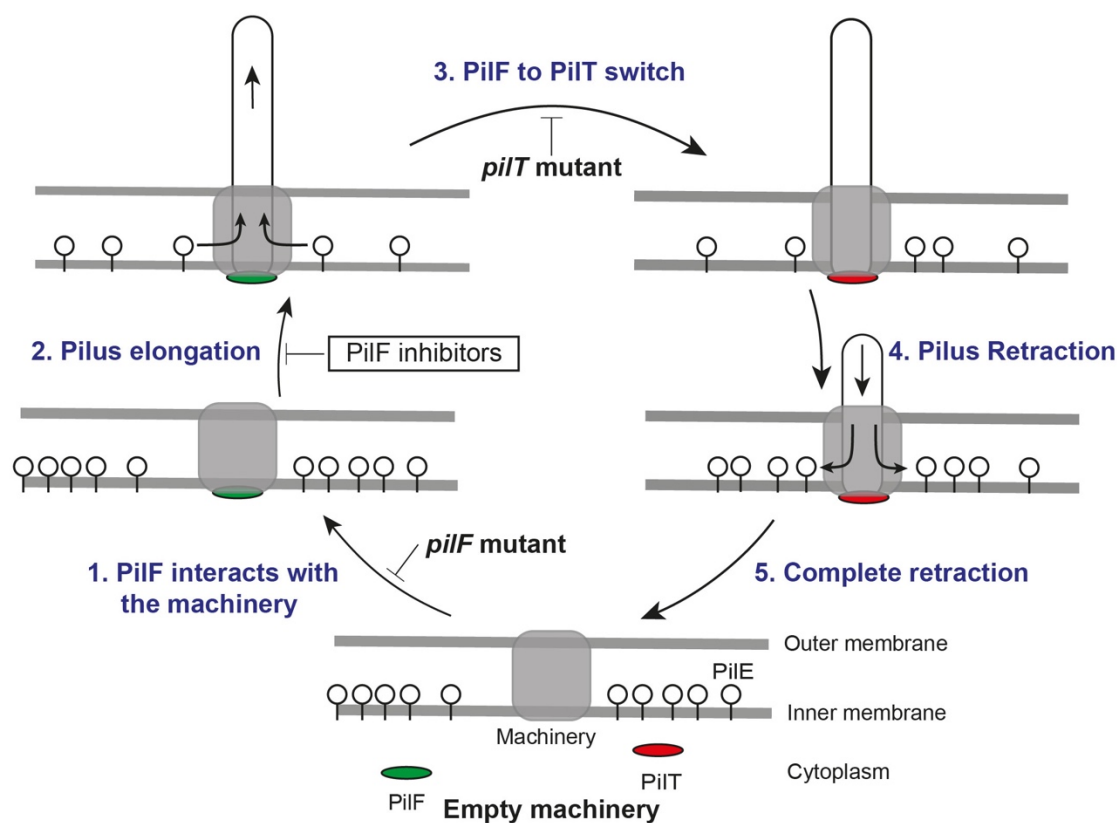


Fig. S3. Schematic representation of the pilus elongation/retraction cycle. Numerous empty piliation machineries can be found on the bacterial surfaces (17), suggesting a resting state where pilin monomers are in the inner membrane and the PilF/T ATPases in the cytoplasm. The piliation cycle is likely initiated with the interaction of PilF with a machinery (step 1). PilF activity then powers assembly of the monomers in a fibre (step 2), and can be inhibited by the hit compounds identified in this study. Then, PilF disengages and PilT comes into play (step 3). Pilus retraction can then take place (step 4), leading to complete retraction (step 5), and the cycle can start again.

Supplementary References

1. Nassif X, *et al.* (1993) Antigenic variation of pilin regulates adhesion of *Neisseria meningitidis* to human epithelial cells. *Mol Microbiol* 8(4):719-725.
2. Kellogg DS, Jr., Cohen IR, Norins LC, Schroeter AL, & Reising G (1968) *Neisseria gonorrhoeae*. II. Colonial variation and pathogenicity during 35 months in vitro. *J Bacteriol* 96(3):596-605.
3. Soyer M, *et al.* (2014) Early sequence of events triggered by the interaction of *Neisseria meningitidis* with endothelial cells. *Cell Microbiol* 16(6):878-895.
4. Schoolnik GK, Fernandez R, Tai JY, Rothbard J, & Gotschlich EC (1984) Gonococcal pili. Primary structure and receptor binding domain. *J Exp Med* 159(5):1351-1370.
5. Wang LC, Litwin M, Sahiholnasab Z, Song W, & Stein DC (2018) *Neisseria gonorrhoeae* Aggregation Reduces Its Ceftriaxone Susceptibility. *Antibiotics (Basel)* 7(2).
6. Schneider CA, Rasband WS, & Eliceiri KW (2012) NIH Image to ImageJ: 25 years of image analysis. *Nat Meth* 9(7):671-675.
7. Imhaus AF & Dumenil G (2014) The number of *Neisseria meningitidis* type IV pili determines host cell interaction. *EMBO J* 33(16):1767-1783.
8. Trott O & Olson AJ (2010) AutoDock Vina: improving the speed and accuracy of docking with a new scoring function, efficient optimization, and multithreading. *J Comput Chem* 31(2):455-461.
9. Morris GM, *et al.* (2009) AutoDock4 and AutoDockTools4: Automated docking with selective receptor flexibility. *J Comput Chem* 30(16):2785-2791.
10. Soding J, Biegert A, & Lupas AN (2005) The HHpred interactive server for protein homology detection and structure prediction. *Nucleic Acids Res* 33(Web Server issue):W244-248.
11. Huang Y & Zhang L (2017) An In Vitro Single-Primer Site-Directed Mutagenesis Method for Use in Biotechnology. *Methods Mol Biol* 1498:375-383.
12. Mehr IJ, Long CD, Serkin CD, & Seifert HS (2000) A homologue of the recombination-dependent growth gene, *rdgC*, is involved in gonococcal pilin antigenic variation. *Genetics* 154(2):523-532.
13. Rule CS, Patrick M, & Sandkvist M (2016) Measuring In Vitro ATPase Activity for Enzymatic Characterization. *J Vis Exp* (114).
14. Harlow E & Lane D (1988) *Antibodies: a laboratory manual*.
15. Schuck P, Perugini MA, Gonzales NR, Howlett GJ, & Schubert D (2002) Size-distribution analysis of proteins by analytical ultracentrifugation: strategies and application to model systems. *Biophys J* 82(2):1096-1111.
16. Brookes E, Cao W, & Demeler B (2010) A two-dimensional spectrum analysis for sedimentation velocity experiments of mixtures with heterogeneity in molecular weight and shape. *Eur Biophys J* 39(3):405-414.
17. Chang YW, *et al.* (2016) Architecture of the type IVa pilus machine. *Science* 351(6278):aad2001.

Replicat #1

Compound coordinate	Compound ID	Batch ID	Inhib. Adhe. (% of ctrl)	# Cell (% of ctrl)	Cpd coordinate	Compound ID	Batch ID	Inhib. Adhe. (% of ctrl)	# Cell (% of ctrl)
004-P024	RA03684572	CL21.003275-1	128.08	101.93	005-B017	A000077521	CL21.004246-1	82.71	93.11
004-N024	A000386933	CL21.003202-1	125.44	110.17	007-M024	A003507184A	F-35978-106-TFA	81.01	108.43
004-B024	CM13735	CM13735-0	122.14	105.23	007-H024	EX00046967	FFT.REX1.030.076	80.55	102.68
004-K024	RA0368656A	CL21.001971E-1	120.99	99.58	007-N023	A003129068	FFT.REX1.028.060	80.22	93.19
004-I024	RA07480876	CL21.001639-1	120.09	91.81	005-K015	SR140174	SR140174-0	80.15	109.19
005-M024	A000074453	CL21.004321-1	116.20	97.25	004-L023	SSR152401	SSR152401-1	79.78	90.63
004-O024	CL21.002170A	CL21.002170A-1	115.64	93.70	006-H020	A000155873	RU50374/21522-107-C	79.36	96.30
005-A024	RA03684253A	CL21.002947F-2	114.30	94.57	007-M023	CL21.003971	CL21.003971-1	79.11	106.13
005-O024	RA03685345	CL21.004403-1	114.06	99.20	007-O023	A003530564A	F-36141-146	78.83	107.86
005-C024	A000119854	CL21.005488-1	112.87	106.51	007-N024	EX00046970	FFT.REX1.030.079	78.29	130.29
005-G024	RA03621580	CL21.002049-2	110.96	92.13	005-P021	SSR116575	SSR116575-1	78.06	111.87
005-D024	SW59004	CL21.002118-1	110.13	92.86	007-A015	SL50.6260-17	SL50.6260-17-A	77.96	121.37
005-K024	SAR272799	CL21.004205-1	109.89	100.91	005-K019	SSR340568	SSR340568-2	77.94	97.49
005-F024	CL21.002143	CL21.002143-1	108.99	90.67	007-I023	A000152820	RU54214/21604-062-A	76.79	105.27
005-J024	RA03521395	CL21.002176-1	108.10	97.49	005-C023	SSR107843	SSR107843-1	76.57	94.81
005-N024	CL21.002240	CL21.002240-1	108.04	114.80	005-L017	RA03688136A	CL21.003146A-1	76.39	107.49
005-P024	CL21.002242	CL21.002242-1	107.09	95.06	006-A021	A000325675D	T007185-1	74.24	100.22
005-I024	RA04019739	CL21.002991-2	106.85	99.20	004-E010	A000499132	LBR2327R	74.24	99.35
007-D017	EX00046908A	FFT.REX1.030.017	104.90	99.80	005-M018	A000074262	CL21.003560-2	73.83	110.90
005-H024	RA05157139	CL21.002165-1	103.87	100.42	007-E023	A003491263A	F-34947-029-3	71.84	113.32
007-B024	EX00046979	FFT.REX1.030.088	102.83	113.90	007-L005	SR241866A	SR241866A-1	71.79	93.47
007-A024	A000185583A	RU749773	102.37	110.73	004-A024	A000391823A	CL21.003237C-1	71.32	99.11
006-D024	A000078147	K954148-E	101.47	96.79	007-P006	RA03683902A	CL21.003020A-1	70.40	122.52
007-A021	SR149076A	SR149076A-0	101.28	131.44	004-I006	SSR133686	SSR133686-2	70.34	123.83
007-P023	A003129155A	FFT.REX1.028.061	98.83	90.89	006-P018	A000163797	S861420-E	70.30	116.64
007-C024	RA07111100	K959425-E	98.59	110.16	007-H023	EX00046808A	FFT.REX1.028.055	70.26	102.97
006-I024	SL48.1365-00	SL48.1365-00-A	96.44	101.45	007-B023	A000521726A	FFT.REX1.028.089	69.91	117.63
007-I024	SAR105650	F-37273-112-2	95.62	121.95	007-K019	A003435970	P-34020-074-1	68.88	96.64
006-F024	A000158335A	RU46433/4	94.24	117.62	004-K018	SR57667B	SL40.0714-08-A	68.76	113.23
006-O024	A000388623	T006955-1	93.81	101.94	005-E006	SR142742	SR142742-0	68.35	107.00
006-N024	A000193517	TM3455	92.17	103.41	006-J019	SAR321213	RU666477/0	68.18	115.41
006-K024	A000388629	T007343-1	91.94	94.59	005-M012	SR80386	SR80386-0	66.86	109.19
006-P024	SSR118331	SSR118331-3	91.56	110.51	005-K010	SAR409202	SW970-0	66.80	99.93
005-L023	RA03685089	CL21.004350-1	90.28	103.83	006-L016	SAR128741	F-34666-001-1675	66.73	103.41
007-G023	A000066892	K967786-E	90.26	106.13	006-L015	A000334600	F-33589-084-SL415	66.02	101.45
007-F024	EX00046981	FFT.REX1.030.090	90.12	96.64	004-L017	A000387031	CA6031A	65.93	108.76
005-C022	SR44144	CL21.001680-2	89.86	102.86	007-J023	A000388431	FFT.REX1.028.056	65.42	110.44
005-B024	RA03683355	CL21.002114-1	89.74	105.78	006-G012	A002647569A	T007549-1	64.85	99.98
007-E024	A000068881	K959544-E	87.65	102.68	005-L009	RA03717047A	CL21.003564A-1	63.76	125.28
007-K023	A000068908	L950537-E	87.62	94.05	006-J007	A000975867	RU22974/RU22974-12	62.41	103.16
007-H018	A000124389	FFT.REX1.028.014	87.35	90.89	005-G019	A003118102A	SL50.6538-10-A	62.33	102.86
007-L023	A000068880	FFT.REX1.028.059	87.16	113.90	006-I018	SW64825	SW64825-XA	62.13	121.30
007-G024	SR140393	SR140393-0	86.72	115.62	007-C023	A000141262	S831343-E	62.05	96.64
007-D024	SAR393590	FFT.REX1.030.089	86.64	131.44	006-K019	A002863473	F-28906-015-0396	61.42	111.49
005-G022	SAR320770	CL21.003184-2	86.35	90.18	005-O022	RA03684796	CL21.003084-2	60.96	107.49
007-D023	EX00046806	FFT.REX1.028.052	85.61	113.61	006-C010	A000436353A	T007373-1	60.91	95.08
007-A023	SL70.0226-24	SL70.0226-24-A	85.44	92.61	006-E019	SAR159550A	SAR159550A-1	60.72	94.59
007-F023	SAR301999	FFT.REX1.028.053	83.21	107.86	005-A022	SAR320933	CL21.003338-2	60.66	99.69
007-J024	EX00046968	FFT.REX1.030.077	83.05	122.81					

Replicat #2

Compound coordinate	Compound ID	Batch ID	Inhib. Adhe. (% of ctrl)	# Cell (% of ctrl)
004-N016	RA03683960A	SW9457-0	106.47	111.46
004-N022	RA03683420A	CL21.003261A-1	105.19	96.10
004-A022	RA03686192	VEM-6141-25B	101.39	93.46
004-A021	EX00046846	FFT.REX1.029.007	99.86	91.34
008-A005	RA06097987	CL21.002080-1	93.38	119.43
004-C011	A003204022A	F-33466-093-1740	90.73	97.96
008-I024	EX00111922A	FFT.REX1.133.091	90.49	90.67
004-N023	SSR139812	SSR139812-1	90.48	113.31
004-L018	SAR321132	CL21.003236-1	90.27	95.04
002-I023	A000388122A	818636A-001	88.84	93.26
004-C016	RA03711872	044018-003	88.38	92.40
006-K020	A000548063	MHT60	88.37	107.37
006-N016	A000365573	104601-001	87.94	121.38
007-N016	A000388726A	FFT.REX1.028.008	87.09	118.23
005-N022	CL21.004793	CL21.004793-1	87.00	90.24
001-A011	SAR109854A	SAR109854A-2	86.23	109.08
007-M022	SR150697	SR150697-1	85.45	129.46
004-J021	A000364254	SL82.0715-00-B	85.30	97.43
004-P022	RA03689183	SL34.0922-00-A	84.84	92.40
002-A011	A002609943	F-33109-138-C	83.60	96.68
007-A012	SAR321044	000473-002	83.07	93.23
004-M022	SAR184370	SL92.0725-00-A	82.54	90.28
004-D021	A000139794A	SW5230-0	82.07	104.84
007-P011	EX00046860	FFT.REX1.029.024	80.84	106.99
008-M014	RA03681856	FFT.REX1.028.022	80.23	90.94
002-N012	SAR111011	K862726-E	78.86	98.97
001-A012	A000187322A	RU71751/26353-085-A	77.47	93.38
004-B015	A000160158	RU44675/2	76.59	100.07
004-L014	RA04321241A	WLS-1602-9-4	76.54	100.87
004-L022	RA03685332	CL21.003245-1	75.67	112.25
004-O012	RA03686365	CM57452-0	74.85	92.66
006-N023	SAR102361A	VAC.HAL1.070	74.04	179.52
004-K008	A001067195	CR11585	71.31	94.25
002-K023	SW35213	SW35213-0	71.06	120.64
006-N017	A001842989A	SL50.6242-10-A	70.81	108.22
004-A016	SSR117249A	SSR117249A-1	70.03	102.72
001-A010	A002287657	S0105170-E	69.10	113.56
006-M022	SR143391A	SR143391A-0	68.85	139.63
008-A009	EX00111885	FFT.REX1.133.053	67.99	100.80
004-C022	A000384853	DRB1158-1	67.37	93.46
004-P017	SAR320783A	CL21.003334A-1	67.11	120.20
004-P018	SAR320870	CL21.003144-1	66.29	104.31
006-M016	SSR134493A	SSR134493A-2	65.56	93.37
006-M020	SR151068	SR151068-1	64.98	142.18
001-M022	A000348503	W028455-E	64.42	91.13
004-P015	A003404030	CL21.003953-1	64.24	135.29
006-L012	RA03687791	CR3926	64.14	90.40
004-E019	A000408915	K9923589-E	63.73	104.84
006-P016	A000066811	K967631-E	63.37	133.69
004-O021	SAR144993	SAR144993-1	62.96	122.31
006-M023	A003572820B	T-1356JM-045-2	62.87	133.69
006-L023	A002243388	F-32966-126	62.34	154.91
008-N015	EX00111835	FFT.REX1.133.002	62.33	132.85
001-A023	A003543309	P-31359-051-1	61.58	94.22
006-K016	SR240253A	SR240253A-1	61.48	112.04
006-M017	A003703869	P-34898-092-1	61.42	91.25
004-M015	RA03688722	SL41.2290-00-A	61.17	114.90
005-K023	SR300408A	SR300408A-2	60.81	125.55
006-M021	SAR408850	T007565-1	60.35	111.19

Replicat #1

&

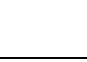
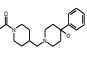
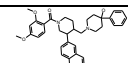
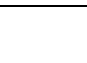
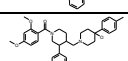
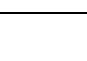
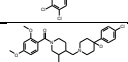
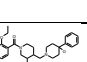
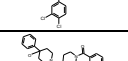
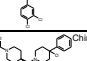
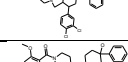
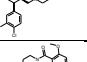
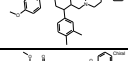
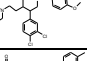
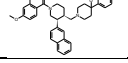
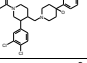

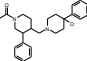
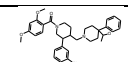

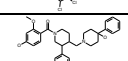
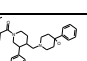
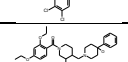
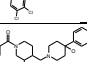
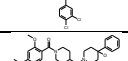
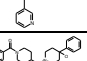
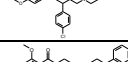
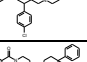
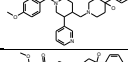
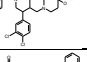
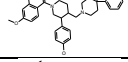
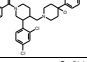
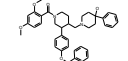
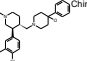
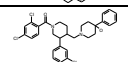


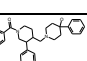
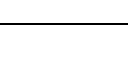
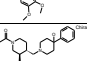
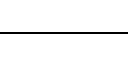
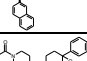
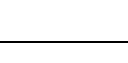
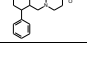
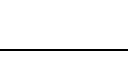
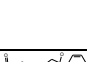

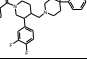
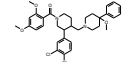
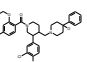
Replicat #2

Compound coordinate	Compound ID	Batch ID	Inhib. Adhe. (% of ctrl)	# Cell (% of ctrl)	Compound coordinate	Compound ID	Batch ID	Inhib. Adhe. (% of ctrl)	# Cell (% of ctrl)
004-D024	RA04244647	FFT.REX1.030.001	97.30	93.46	004-D024	RA04244647	FFT.REX1.030.001	66.34	90.54
007-K024	A000068853	K959512-E	95.32	108.72	007-K024	A000068853	K959512-E	92.26	122.44
004-E009	A000550256	LGK5282	88.40	119.83	004-E009	A000550256	LGK5282	74.13	97.43
007-B011	A000366755	FFT.REX1.028.074	80.74	102.10	007-B011	A000366755	FFT.REX1.028.074	85.57	99.69
006-B009	SAR111018	013407-001	80.11	111.49	006-B009	SAR111018	013407-001	69.12	103.13
006-H023	SAR112000A	F-33712-054-330	73.77	90.91	006-H023	SAR112000A	F-33712-054-330	62.90	144.30
004-P014	SL50.4526-00	SL50.4526-00-A	62.15	122.65	004-P014	SL50.4526-00	SL50.4526-00-A	68.96	103.52

Supplementary Table 1. List of the selected hits according to the two replicates of the primary screen. Highlighted in bold are compounds used for further investigation.

Compound coordinate	Compound ID	Batch ID	IC50 (M)	TC50 (M)	Selected compound
004-E009	A000550256	LGK5282	1,19E-08	3,70E-06	
006-M017	A003703869	P-34898-092-1	7,20E-09	8,29E-06	A
007-L005	SR241866A	SR241866A-1	1,73E-08	7,83E-06	B
004-K018	SR57667B	SL40.0714-08-A	5,03E-07	>3.00E-05	
004-N023	SSR139812	SSR139812-1	5,21E-06	1,72E-05	
004-P022	RA03689183	SL34.0922-00-A	1,24E-05	>3.00E-05	
005-A022	SAR320933	CL21.003338-2	1,57E-05	1,64E-05	
005-K015	SR140174	SR140174-0	2,07E-06	>3.00E-05	
005-K023	SR300408A	SR300408A-2	3,25E-06	2,10E-05	
006-K016	SR240253A	SR240253A-1	8,45E-06	>3.00E-05	
006-L016	SAR128741	F-34666-001-1675	3,36E-06	>3.00E-05	
006-L023	A002243388	F-32966-126	5,21E-06	1,11E-05	
006-M023	A003572820B	T-1356JM-045-2	9,32E-06	2,02E-05	
007-D017	EX00046908A	FFT.REX1.030.017	1,42E-05	2,16E-05	
007-H018	A000124389	FFT.REX1.028.014	3,98E-07	>3.00E-05	
008-A009	EX00111885	FFT.REX1.133.053	2,66E-07	1,98E-05	C
001-M022	A000348503	W028455-E	4,02E-07	NoVal	
004-A016	SSR117249A	SSR117249A-1	1,01E-06	1,33E-05	
004-A021	EX00046846	FFT.REX1.029.007	6,37E-07	5,73E-06	
004-B015	A000160158	RU44675/2	NoVal	NoVal	
004-C022	A000384853	DRB1158-1	NoVal	NoVal	
004-D024	RA04244647	FFT.REX1.030.001	NoVal	NoVal	
004-I006	SSR133686	SSR133686-2	3,80E-07	2,71E-05	
004-J021	A000364254	SL82.0715-00-B	NoVal	1,46E-05	
004-K008	A001067195	CR11585	NoVal	<1.00E-09	
004-M022	SAR184370	SL92.0725-00-A	NoVal	NoVal	
004-N016	RA03683960A	SW9457-0	NoVal	NoVal	
004-O021	SAR144993	SAR144993-1	1,24E-06	1,63E-05	
005-B017	A000077521	CL21.004246-1	NoVal	6,40E-06	
005-C022	SR44144	CL21.001680-2	1,12E-05	NoVal	
005-C023	SSR107843	SSR107843-1	2,68E-06	NoVal	
005-E006	SR142742	SR142742-0	NoVal	7,93E-06	
005-G019	A003118102A	SL50.6538-10-A	6,02E-05	NoVal	
005-G022	SAR320770	CL21.003184-2	NoVal	NoVal	
005-K010	SAR409202	SW970-0	4,28E-07	NoVal	
005-K019	SSR340568	SSR340568-2	2,28E-03	NoVal	
005-L009	RA03717047A	CL21.003564A-1	3,07E-07	NoVal	
005-L017	RA03688136A	CL21.003146A-1	NoVal	4,63E-07	
005-L023	RA03685089	CL21.004350-1	NoVal	NoVal	
005-M012	SR80386	SR80386-0	NoVal	NoVal	
005-M018	A000074262	CL21.003560-2	NoVal	NoVal	
005-N022	CL21.004793	CL21.004793-1	NoVal	9,31E-07	
005-P021	SSR116575	SSR116575-1	NoVal	NoVal	
006-A021	A000325675D	T007185-1	NoVal	NoVal	
006-C010	A000436353A	T007373-1	NoVal	NoVal	
006-E019	SAR159550A	SAR159550A-1	2,63E-07	NoVal	
006-G012	A002647569A	T007549-1	NoVal	NoVal	
006-L015	A000334600	F-33589-084-SL415	1,47E-05	NoVal	
006-P018	A000163797	S861420-E	NoVal	NoVal	
007-A015	SL50.6260-17	SL50.6260-17-A	NoVal	>3.00E-05	
007-A021	SR149076A	SR149076A-0	6,75E-07	4,88E-06	
007-B011	A000366755	FFT.REX1.028.074	NoVal	2,93E-05	
007-K019	A003435970	P-34020-074-1	NoVal	4,54E-06	
007-L023	A000068880	FFT.REX1.028.059	NoVal	5,33E-06	
007-M022	SR150697	SR150697-1	NoVal	NoVal	
007-N016	A000388726A	FFT.REX1.028.008	NoVal	>3.00E-05	
007-P006	RA03683902A	CL21.003020A-1	NoVal	NoVal	
008-A005	RA06097987	CL21.002080-1	NoVal	7,54E-07	
008-M014	RA03681856	FFT.REX1.028.022	NoVal	NoVal	

Supplementary Table 2. Summary of compound IC50 and TC50.

Derivative #	Compound ID	Structure	Aggregation Index		Derivative #	Compound ID	Structure	Aggregation Index	
			Replicat #1	Replicat #2				Replicat #1	Replicat #2
Ctrl		-	1	1	624	SR126808A		0,89094713	0,648688
DMSO		-	1,16830336	1,00435496	625	SR126739		1,54600459	0,89671185
Compound B	SR241866A		0,609719962	0,209864961	626	SR126312A		1,22775082	0,87872452
601	SR126893A		0,42650228	0,238486	627	SR140306A		0,98612276	0,46759953
602	SR126546A		0,6053085	0,30650501	628	SR242124A		1,05299651	0,73469891
603	SR140314A		0,38375214	0,23748919	629	SR126115A		1,23409329	0,63098143
604	SR242079A		0,287558758	0,045618314	630	SR140485A		0,85645871	0,64356534
605	SAR151679		0,465438758	0,139783739	631	SR126892A		1,07113654	0,54691496
606	SR242462A		1,25962819	0,50913406	632	SR126361A		0,31061435	0,26296693
607	SR126178A		0,62000633	0,41835116	633	SR48388A		1,73185865	0,88282017
608	SR126695		0,197078267	0,064090347	634	SR242670A		0,54000576	0,44420974
609	SR242125A		0,6275706	0,28925333	635	SR126452A		1,38475325	0,81541015
610	SR126427A		0,42663094	0,26064471	636	SR126699A		0,195803394	0,126080336
611	SR126451A		0,90147473	0,4911623	637	SR126809A		0,59490547	0,36320443
612	SR242160A		0,80604821	0,51638437	638	SR126453A		0,57259999	0,3294846
613	SR242251A		0,010377469	0,022667427	639	SR126127A		0,3742833	0,32088924
614	SR241996		0,51236946	0,37941988	640	SR126441A		1,03341264	0,58891034
615	SR241972A		0,345815415	0,191877005	641	SR241865A		0,69140818	0,45331895
616	SR49220A		0,78577057	0,51905737	642	SAR151678		0,113274088	0,150259685
617	SR126442A		0,87757807	0,45620599	643	SR126362A		1,1768149	0,55701683
618	SR140712A		1,56908561	0,62796268	644	SR126837A		0,96325619	0,76704886
619	SR241781A		0,83481654	0,59867234	645	SR241956A		0,84378233	0,63609224
620	SR126650		1,20296372	0,60560303	646	SR126859A		0,45885153	0,33970585
621	SR241864A		0,238777312	0,109675625	647	SR242463A		1,05178961	0,87111127
622	SR241973A		0,87266368	0,53949866	648	SR126128A		0,209899286	0,141109329
623	SR126651A		0,90151358	0,84871816	649	SR241866A		0,156063497	0,163443338

Supplementary Table 3. Structure activity relationship of Compound B.

Highlighted in green or red are derivatives with a better or a worst inhibition activity than compound B, respectively.